bioRxiv preprint doi: https://doi.org/10.1101/2020.02.24.962829; this version posted February 26, 2020. The copyright holder for this preprint (which was not certified by peer review) is the author/funder, who has granted bioRxiv a license to display the preprint in perpetuity. It is made available under aCC-BY 4.0 International license.

Ecdysone steroid hormone remote controls intestinal stem cell fate decisions via the *PPARγ*-homologue *E75B* in *Drosophila*.

Lisa Zipper[1], Denise Jassmann[1], Bastian Görlich[1] and Tobias Reiff[1,2]

[1]Institute of Genetics, Heinrich-Heine-University, Universitätsstr. 1, Düsseldorf, Germany
[2]Author for correspondence: Tobias Reiff, Institute of Genetics, Heinrich-Heine-University, reifft@hhu.de

Abstract (150 words)

Developmental studies revealed fundamental principles on how organ size and function is achieved, but less is known about organ adaptation to new physiological demands. In fruit flies, juvenile hormone induces intestinal stem cell (ISC) driven absorptive epithelial expansion balancing energy uptake with increased energy demands of pregnancy.

Here, we show 20-Hydroxy-Ecdysone (20HE)-signaling controlling organ homeostasis with physiological and pathological implications. Upon mating, ovarian 20HE acts on nearby midgut progenitors inducing *Ecdysone-induced-protein-75B (E75B).* Strikingly, the *PPARγ*-homologue *E75B* restricts ISC daughter cell differentiation towards absorptive enterocyte lineage ensuring epithelial growth even in the absence of local fate determining Notch. To our knowledge, this is the first time a systemic hormone is shown to direct local stem cell fate decisions. Given the protective, but mechanistically unclear role of steroid hormones in female colorectal cancer patients, our findings suggest a tumor-suppressive role for steroidal signalling by promoting postmitotic fate independent of deteriorated local signalling.

bioRxiv preprint doi: https://doi.org/10.1101/2020.02.24.962829; this version posted February 26, 2020. The copyright holder for this preprint (which was not certified by peer review) is the author/funder, who has granted bioRxiv a license to display the preprint in perpetuity. It is made available under aCC-BY 4.0 International license.

Introduction

Reproduction is an energetically costly process triggering multiple physiological adaptations of organs such as liver, pancreas and gastrointestinal tract upon pregnancy in various species (Hammond 1997, Roa & Tena-Sempere 2014). As a part of the hormonal response to mating and increased metabolic energy consumption, the female *Drosophila melanogaster* gut is remodeled in size and physiology by stimulating intestinal stem cell (ISC) driven epithelial expansion to achieve an even energy balance (Cognigni et al 2011, Klepsatel et al 2013, Reiff et al 2015).

Since the discovery of adult intestinal stem cells (Micchelli & Perrimon 2006, Ohlstein & Spradling 2006), local signaling pathways such as Notch (N), Jak/Stat, EGFR, Wnt/wingless, Insulin-receptor, Hippo/Warts and Dpp-signaling were shown to contribute to intestinal homeostasis under physiological and challenged conditions like bacterial infections (Miguel-Aliaga et al 2018)(and references therein). The midgut epithelium is maintained by ISC giving rise to only two types of differentiated cells: enteroendocrine cells (EE) and absorptive enterocytes (EC). Pluripotent ISC are able to self-renew or divide asymmetrically to give rise to committed EC precursor cells called enteroblasts (EB) and enteroendocrine precursor (EEP) cells, which upon timely activation of *scute* in ISC divide once more prior to terminal differentiation yielding a pair of EE (Chen et al 2018, Micchelli & Perrimon 2006, Ohlstein & Spradling 2006, Ohlstein & Spradling 2007). Nine out of ten ISC mitosis give rise to EB specified by N-activation in EB daughters (Micchelli & Perrimon 2006, Ohlstein & Spradling 2006, Ohlstein & Spradling 2007). However, post-mitotic EB retain a certain degree of plasticity by: (1) delaying their terminal differentiation through mesenchymal-to-epithelial transition (MET) (Antonello et al 2015a), (2) changing their fate to EE upon loss of lineage marker *klu* (*klumpfuss*) and (3) undergoing apoptosis as an additional homeostatic mechanism (Korzelius et al 2019, Reiff et al 2019).

Apart from local signaling pathways, systemically released JH is able to control ISC proliferation through heterodimers of *Met (methoprene-tolerant)* and *gce (germ cells expressed)* nuclear hormone receptors upon mating (Reiff et al 2015). JH coordinates *Drosophila* larval development in concert with the steroid hormone 20-hydroxy-ecdysone (20HE) (Bownes et al 1984, Gilbert et al 2002). In adult female flies, 20HE is released by the ovary and its titer increases upon mating (Ameku & Niwa 2016, Gilbert & Warren 2005, Harshman et al 1999), prompting us to investigate the Ecdysone-receptor (EcR) signaling cascade in organ plasticity during reproduction in the anatomically proximal posterior midgut (PMG). Downstream of EcR activation, we found upregulation of *Ecdysone-induced protein 75B (E75B)* splice variants ensuring absorptive EC production upon mating. Using the established Notch tumor paradigm, we found that 20HE remote controls EB differentiation independently of local fate determining Notch. The mechanism identified in this study not only plays a role in the physiology of mating, but also contributes to our understanding of the protective effects of steroid hormone signaling in the pathophysiology of human colorectal cancer.

bioRxiv preprint doi: https://doi.org/10.1101/2020.02.24.962829; this version posted February 26, 2020. The copyright holder for this preprint (which was not certified by peer review) is the author/funder, who has granted bioRxiv a license to display the preprint in perpetuity. It is made available under aCC-BY 4.0 International license.

Results

EcR controls intestinal stem cell proliferation and progenitor differentiation

The female fly intestine undergoes various physiological post-mating adaptations including a size increase of the absorptive epithelium (Cognigni et al 2011, Klepsatel et al 2013, Reiff et al 2015). Intrigued by post-mating increases of 20HE titers (Ameku & Niwa 2016, Harshman et al 1999), we explored a role for EcR-signaling in mating adaptations of the adult *Drosophila melanogaster* intestine.

EcR encodes for three different splice variants: *EcR.A, EcR.B1* and *EcR.B2* (Cherbas et al 2003, Talbot et al 1993), which we detected by PCR in intestinal tissue with highest expression for *EcR.B2* (Fig.S1B). Using pan-EcR antibodies, we found EcR in ISC (positive for the Notch ligand Delta^{+}), EB (Notch responsive element, NRE-GFP^{+}) and EC (Discs-large-1, Dlg-1^{+}, Fig.S1C-F'''). To investigate a role for the EcR in intestinal tissue homeostasis, we first manipulated EcR function in ISC and EB using the *'ReDDM'* (Repressible Dual Differential Marker, Fig.S1A) tracing method to observe its overall impact on tissue renewal (Antonello et al 2015a). Briefly, *ReDDM* differentially marks cells having active or inactive *Gal4* expression with fluorophores of different stability. Combined with the enhancer trap *esg-Gal4,* active in progenitors (ISC and EB), *esg^{ReDDM}* double marks ISC and EB driving the expression of *UAS-CD8::GFP* (*>CD8::GFP*) with short half-life and *>H2B::RFP* with long half-life. Upon epithelial replenishment, newly differentiated EC and EE stemming from ISC divisions retain a RFP^{+}-nuclear stain due to fluorophore stability (Antonello et al 2015a). Crosses are grown at 18°C in which transgene expression is repressed by ubiquitous tubulin-driven temperature sensitive Gal80^{ts}. By shifting adult females to 29°C, Gal80^{ts} is destabilized, in turn enabling spatiotemporal control of *esg^{ReDDM}*-tracing and additional UAS-driven transgenes in progenitors (Fig.S1A).

After seven days of tracing control virgin females (VF, Fig.1B) and mated females (MF, Fig.1C) using *esg^{ReDDM}* show increases progenitor numbers (Fig.1G) and newly generated EC (Fig.1H) in the R5 region of the PMG confirming previous observations (Reiff et al 2015). Reducing *EcR*-levels with two different *>EcR-RNAi* stocks in MF resulted in a reduction of ISC/EB numbers (Fig.1D,G,S1K) and newly generated EC (Fig.1D,H,S1K) to levels comparable to VF controls (Fig.1B,G,H). We addressed knockdown efficiency of *>EcR-RNAi* in *esg^{ReDDM}* by staining with EcR-antibodies and measuring fluorescence intensity of progenitor cells *in situ* and found EcR-signal significantly decreased in both RNAi lines (Fig.S1G).

Independent of EcR-abundance, we found that expressing dominant-negative *EcR.B2* isoforms or *EcR*-heterozygosity using *EcR^{M554fs}*, a well described loss-of-function (LOF) allele, phenocopy *>EcR-RNAi* (Fig.S1H,I,J). Generally, *EcR* LOF leads to a similar phenotype as JH-receptor knockdown in MF (Reiff et al 2015). To investigate whether EcR-levels affect progenitor behavior, we overexpressed wildtype *EcR.B2* and *pan-EcR* using *esg^{ReDDM}* in VF. We found neither induction of progenitor numbers nor an increase in new EC (Fig.1E,F,G,H), suggesting that EcR-dependent proliferation and differentiation of progenitors might be limited by 20HE availability (Fig.1I).

bioRxiv preprint doi: https://doi.org/10.1101/2020.02.24.962829; this version posted February 26, 2020. The copyright holder for this preprint (which was not certified by peer review) is the author/funder, who has granted bioRxiv a license to display the preprint in perpetuity. It is made available under aCC-BY 4.0 International license.

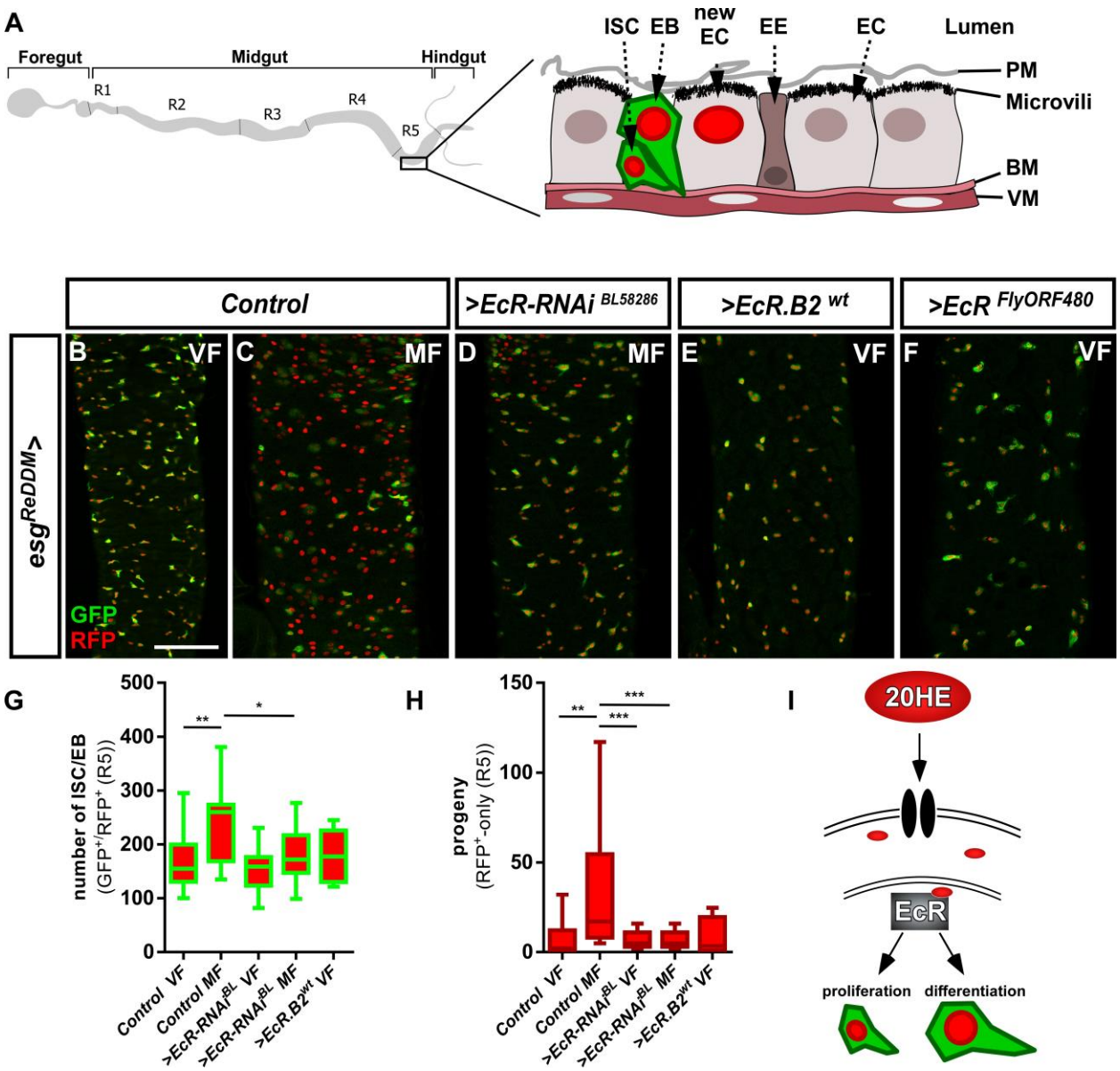

Figure 1. The Ecdysone receptor in intestinal progenitors controls tissue homeostasis

(A) Scheme of the adult *Drosophila melanogaster* gastrointestinal tract with cartoon depicting the midgut epithelial monolayer composed of intestinal stem cells (ISC), enteroblasts (EB), enterocytes (EC) and enteroendocrine cells (EE) colored according to the lineage tracing system ReDDM with esg-Gal4 explained in more detail in Fig.S1 and (Antonello et al 2015a). Posterior midguts (PMG) after seven days of esg^{ReDDM} tracing of control (crossed with w^{1118}) adult MF (C) show mating dependent addition of new EC compared to control VF (B,G,H) (Reiff et al 2015). (D) Knock-down of EcR using UAS-driven RNAi abolishes mating induced new EC generation in MF. (E+F) Overexpression of *>EcR.B2* in VF (E) and $>EcR^{FlyORF840}$ (F) does not induce proliferation or differentiation of progenitors (ISC+EB). (G-I) Quantification of progenitor numbers (G) and traced progeny encompassing EC and EE (H) in R5 PMG (n=24,17,17,17, 8). Error bars are Standard Error of the Mean (SEM) and asterisks denote significances from one-way ANOVA with Bonferroni's Multiple Comparison Test (* p<0.05, ** p<0.01; *** p<0,001). (I) Cartoon depicting experimental manipulations on EcR signalling pathway investigated with esg^{ReDDM}. Scale bars = 100µm

bioRxiv preprint doi: https://doi.org/10.1101/2020.02.24.962829; this version posted February 26, 2020. The copyright holder for this preprint (which was not certified by peer review) is the author/funder, who has granted bioRxiv a license to display the preprint in perpetuity. It is made available under aCC-BY 4.0 International license.

Ecdysone is increased upon mating and actively transported into progenitors to adapt intestinal physiology to pregnancy

20HE is a polar steroid dispersing through hemolymph binding to EcR to activate target gene transcription (Bownes et al 1984, Gilbert et al 2002). As orally administered 20HE is metabolized and cleared of rapidly, we used the potent non-steroidal EcR agonist RH5849, developed and used as pest control due to its stability, specificity and a 30-60 times higher efficacy compared to 20HE (Robinson et al 2008, Robinson et al 1987, Wing et al 1988). Testing concentrations from 1-100µg/ml, we observed expected larval molting defects for concentrations from 50µg/ml upwards in timed egg-layings (Fig. S2A). Feeding control esg^{ReDDM} VF 50µg/ml RH5849, we traced intestinal progenitors with pharmacologically activated EcR-signaling for seven days. RH5849 strongly induces ISC mitosis, reflected by an tenfold increase in newly generated progeny over mating induction (Fig.2A-C,K). Interestingly, RH5849 mediated EcR-activation leads to no accumulation of progenitors (Fig.2J) as observed in oncogenic manipulations or disruptions of intestinal homeostasis, suggesting a role for EcR in both, proliferation and differentiation (Antonello et al 2015a, Chen et al 2016, Patel et al 2015, Reiff et al 2019). Given the role of 20HE induced programmed cell death (PCD) in larval metamorphosis and the recently discovered role of EB PCD in adult midgut homeostasis (Jiang et al 1997, Jiang et al 2000, Reiff et al 2019), we addressed PCD by activated caspase-3 staining, but found no increase of PCD by RH5849 (data not shown).

In close anatomical proximity to the PMG, the ovaries are an established source for 20HE and ecdysteroidogenesis increases upon mating (Ameku & Niwa 2016, Harshman et al 1999). Using an established reporter for 20HE signaling activation, we found similar increases in the PMG and ovaries (Fig.2H). Cellular 20HE uptake was recently shown to depend on *Ecdysone Importer (EcI)* belonging to the evolutionary conserved SLCO superfamily of solute carrier transporters. *EcI* LOF causes phenotypes indistinguishable from 20HE and *EcR* deficiencies *in vivo* (Okamoto et al 2018). To investigate a role of EcI, we confirmed membrane localization of *>EcI* tagged with HA by immunostaining in progenitors using esg^{ReDDM} (Fig.S2B). After seven days, forced expression of *>EcI* using esg^{ReDDM} in VF lead to no increase in progenitor numbers and new EC, underlining that VF 20HE levels are low (Fig.2D,J,K). Further supporting this hypothesis, *>EcI* in MF lead to an increase of newly generated EC exceeding typical mating induction of MF controls by 4.8 fold (Fig.2E,J,K). Blocking 20HE uptake by *EcI-RNAi* abolished ecdysone induced tissue expansion to VF control levels (Fig.2F,G,J,K). Both, pharmacological and genetic experiments, suggest that 20HE levels and import control EcR-activity upon mating (Fig.2I).

Since we observed EcR in EC (Fig. S1C-F), we investigated its function in this cell type as it has previously been shown that mating through JH-signaling induces not only size adaptations through ISC proliferation, but also metabolic changes in absorptive EC by activating *sterol regulatory element-binding protein* (*Srebp*) upregulating lipid uptake (Reiff et al 2015). We addressed Srebp-activity using a GFP-reporter that reflects upregulation of lipid uptake gene expression (Athippozhy et al 2011, Reiff et al 2015) and confirmed previous observations showing a 2.2 fold increase in *Srebp*-activity (mean fluorescence intensity, Fig.S2C,D) (Reiff et al 2015). MF-flies with *EcR*-knockdown fail to induce *Srebp*-activity over VF controls (Fig.S2E-F,H), whereas feeding VF with RH5849 induced *Srebp*-activity 2.4 fold (Fig.S2G,H).

These data support the idea that mating related synergistic effects of JH- and 20HE-signalling drive changes of intestinal homeostasis and physiology. The JH-signal is transduced by the transcription factor *Krüppel-homolog 1 (Kr-h1)* in adult MF intestines, which prompted us to explore a function for the 'classical' Ecdysone target genes (Jindra et al 2013, Reiff et al 2015).

bioRxiv preprint doi: https://doi.org/10.1101/2020.02.24.962829; this version posted February 26, 2020. The copyright holder for this preprint (which was not certified by peer review) is the author/funder, who has granted bioRxiv a license to display the preprint in perpetuity. It is made available under aCC-BY 4.0 International license.

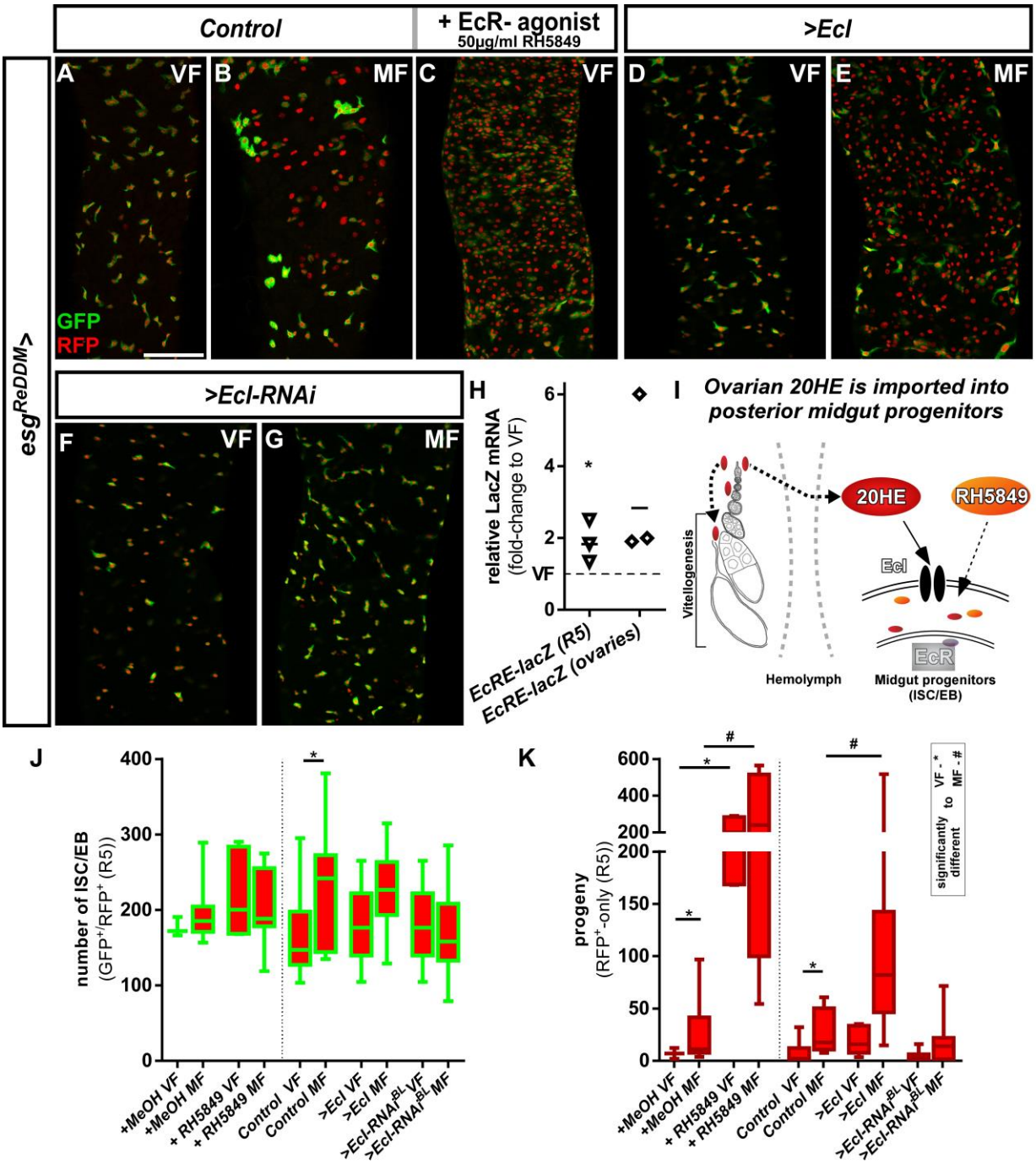

Figure 2. Intracellular 20-Hydroxy-ecdysone levels control ecdysone response through the ecdysone importer

(A+B) Representative adult PMG after seven days of *esg*^{ReDDM} tracing of control VF (A) and MF (B). (C) Control VF PMG after oral administration of RH5849 (50µg/ml) and seven days of tracing. (D-G) Up- and downregulation of *Ecl* in VF (D,F) and MF (E,G) using UAS driven transgenes after seven days of tracing with *esg*^{ReDDM}. Quantitative RT-PCR on *EcRE* (Ecdysone responsive elements, (Schwedes et al 2011)) driving lacZ expression on intestinal cDNA from VF and MF control flies. Values are normalized to VF levels (horizontal line = 1) and statistically analysed using student´s t-test (* p<0.05, ** p<0.01; *** p<0,001;). (I) Cartoon depicting ovarian 20HE release and specific genetical and pharmacological manipulations on EcR signalling pathway in adjacent PMG ISC/EB. (J,K) Quantification of progenitor numbers (J) and traced progeny encompassing EC and EE (K) in R5 PMG (n=3,9,5,13/16,13,8,10,10,19). Error bars are Standard Error of the Mean (SEM) and asterisks denote significances from one-way ANOVA with Bonferroni's Multiple Comparison Test (* p<0.05, ** p<0.01; *** p<0,001; **** p<0.0001). Scale bars = 100µm

bioRxiv preprint doi: https://doi.org/10.1101/2020.02.24.962829; this version posted February 26, 2020. The copyright holder for this preprint (which was not certified by peer review) is the author/funder, who has granted bioRxiv a license to display the preprint in perpetuity. It is made available under aCC-BY 4.0 International license.

Ecdysone-induced protein 75B splice variants control ISC proliferation and enteroblast differentiation

During *Drosophila* development, 20HE pulses lead to binding of EcR directly to regulatory regions of early ecdysone response genes *Ecdysone-induced protein 74A (E74A)* and *E75B* (Bernardo et al 2014, Karim & Thummel 1991, Segraves & Hogness 1990) (Fig.3A). First, we performed conventional PCR to analyse JH- and Ecdysone target gene expression. Signal for *Kr-h1-A (Kr-h1* in the following), but not *Kr-h1-B*, and for all splice variants of *E74A* and *E75B* was found (Fig.3B). Using quantitative real time PCR (qPCR) analysis, we confirmed an increase of JH-pathway activity upon mating using *Kr-h1* as control (Fig.3C) (Reiff et al 2015). To our surprise, we found *E74A* expression unchanged, in contrast to its prominent role in the control of germline stem cell (GSC) proliferation in oogenesis (Ables & Drummond-Barbosa 2010). Instead, we found induction of *E75B-A* and *-C* splice variants (Fig.3C). *E75B* encodes for three protein isoforms (E75B-A, -B and –C) that differ in their N-terminal domain structure (Segraves & Hogness 1990) and E75B-B lacks one of the two zinc-finger DNA binding domains rendering it incapable of direct DNA binding (White et al 1997).

Intrigued by mating increases of *E75B-A/-C* levels, we manipulated E75B function using esg^{ReDDM}. Reducing *E75B* levels with RNAi, we found a significant increase in ISC and EB numbers (Fig.3D,E,I), but not in EC generation compared to VF controls (Fig.3J). In MF, *E75B* knockdown reduced newly generated EC compared to MF controls, pointing to a role of *E75B* in EB differentiation downstream of EcR-activation (Fig.3E,J). Additionally, we investigated homozygous *E75B-A* mutants using MARCM clonal analysis with a known LOF allele (Rabinovich et al 2016). MARCM clones of *E75B-A* ($E75^{A81}$) are significantly larger compared to controls (Fig.S4A-D) and contain few clonal EC (GFP^+/$Dlg\text{-}1^+$, Fig.S4C) reflecting disturbed differentiation (Lee & Luo 1999). Notably, we did not detect EE in *E75B-A* clones by co-staining for the EE-marker prospero (GFP^+/$pros^+$, arrowheads Fig.S4C). These LOF experiments hint to a role for mating induced *E75B-A/-C* splice variants in differentiation of progenitors downstream of EcR.

Forced expression of E75B splice variants with esg^{ReDDM} resulted in three prominent phenotypes: (1) *E75B-A* and *E75B-C* strongly drive differentiation into EC ($Dlg\text{-}1^+$, Fig.3F,H,J) depleting the entire progenitor pool (Fig.3F,H,I). (2) The *E75B-B* isoform induces ISC proliferation in VF (Fig 3G) and raised progenitor numbers suggesting slowed down but not inhibited terminal differentiation (Fig.3G,I,J). (3) All E75B manipulations block EE differentiation (Fig.S4A) possibly reflecting a general block for *E75B-RNAi* and *E75B-B* isoform (Fig.3E,G), whereas *E75B-A* and *E75B-C* instantaneously drive progenitors into EC differentiation preventing further ISC division and thus EE differentiation (Fig.3I,J). Manipulating tissue homeostasis alters midgut length (Hudry et al 2016) and in line with this, E75B manipulations also reduce midgut length by either slowing down terminal differentiation (*E75B-B* and *E75B-RNAi*) or depleting the progenitor pool (*E75B-A*/*–C*, Fig.3K). These findings strongly suggest a role for *E75B* in EB differentiation.

After initial N specification, EB lineage is maintained by the N target *klumpfuss* (*klu*). klu^+-EB retain some plasticity to change fate to EE upon reduction of *klu*-levels (Korzelius et al 2019, Reiff et al 2019). We used klu^{ReDDM} to explore the function of *EcR* and *E75B* in EB lineage identity (Fig.S4B). No changes in EB fate were observed upon knockdown of *EcR* and *E75B* (Fig.S4A,C-E). *E75B-A* and *E75B-C* expression with klu^{ReDDM} phenocopied EB differentiation effects observed in esg^{ReDDM} (Fig.S4H,J,K,L) without non-autonomously inducing proliferation in wild-type ISC of VF and MF (Fig.S4K,L). Expressing *E75B-B* in klu^{ReDDM} lead to delayed EB differentiation similar to esg^{ReDDM} and non-autonomous induction of ISC mitosis (Fig.3G,

bioRxiv preprint doi: https://doi.org/10.1101/2020.02.24.962829; this version posted February 26, 2020. The copyright holder for this preprint (which was not certified by peer review) is the author/funder, who has granted bioRxiv a license to display the preprint in perpetuity. It is made available under aCC-BY 4.0 International license.

Fig.S4I, Fig.S4M) (Patel et al 2015, Reiff et al 2019). Having identified *E75B-A/-C* as mating induced differentiation effector of 20HE signaling, we hypothesized and investigated a synergism of 20HE and JH hormonal signaling pathways controlling epithelial expansion upon mating.

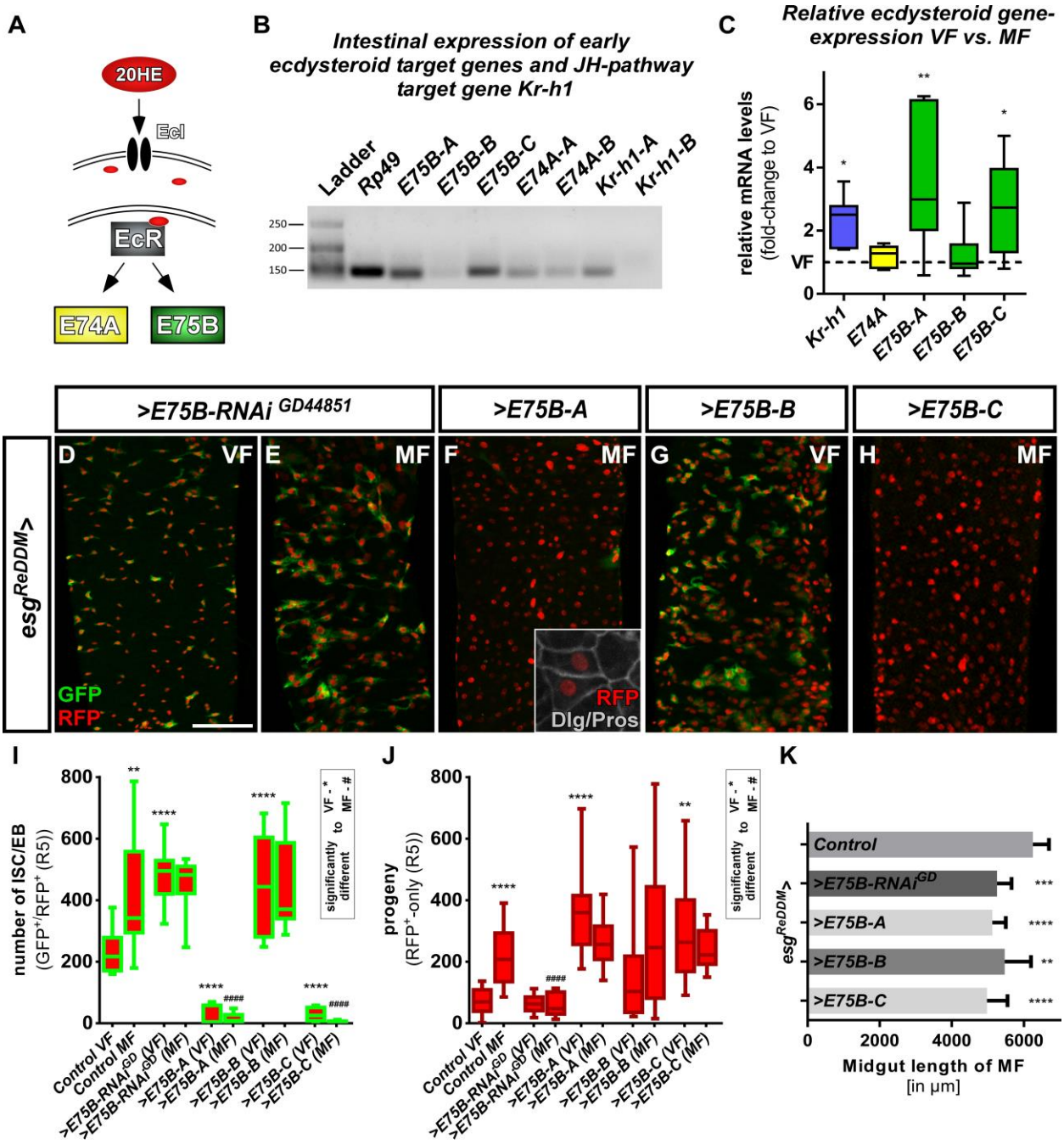

Figure 3. *Ecdysone induced protein 75B* is upregulated upon mating and controls progenitor differentiation

(A) Cartoon depicting EcR signalling cascade activating early ecdysteroid target genes. (B) Expression analysis of Ecdysone- and JH-signaling target genes including splice variants on cDNA transcribed from mRNA isolations from whole midgut dissections of MF. (C) Quantitative RT-PCR on early ecdysteroid genes on intestinal cDNA from VF and MF control flies. Values are normalized to VF levels (horizontal line = 1) and statistically analysed using student´s t-test (n=6; * p<0.05, ** p<0.01; *** p<0,001;). (D-E) RNAi-mediated downregulation of *E75B* in VF (D) and MF (E) after seven days of tracing with *esg*^{ReDDM}. (F-H) Representative images of adult PMG with forced expression of *E75B* splice variants *E75B-A* (F)*, E75B-B* (G) and *E75B-C* (H) after seven days of tracing with *esg*^{ReDDM}. Inset in (F) depicts epithelial integration of newly generated Dlg-1^{+}/RFP^{+}-EC. (I-J) Quantification of progenitor numbers (I) and traced progeny encompassing EC and EE (J) in R5 PMG (n=12,13,10,12,11,14,8,10,10,10). Error bars are Standard Error of the Mean (SEM) and asterisks denote significances from one-way ANOVA with Bonferroni's Multiple Comparison Test (* p<0.05, ** p<0.01; *** p<0,001; **** p<0.0001, identical p-values are marked by # when compared to MF). (K) Overall length in µm of midguts from proventriculus to mid-/hindgut boundary of indicated genotypes. Scale bars = 100µm

bioRxiv preprint doi: https://doi.org/10.1101/2020.02.24.962829; this version posted February 26, 2020. The copyright holder for this preprint (which was not certified by peer review) is the author/funder, who has granted bioRxiv a license to display the preprint in perpetuity. It is made available under aCC-BY 4.0 International license.

The interplay between JH and 20HE in intestinal progenitors

Our data suggests that mating induced JH and 20HE signaling may sequentially affect ISC proliferation and EB differentiation through their effectors *Kr-h1* and *E75B* (Fig.4A) (Reiff et al 2015). In VF lacking mating induction of both hormones (Ameku & Niwa 2016, Harshman et al 1999, Reiff et al 2015), forced *>Kr-h1* expression crossed to esg^{ReDDM} doubles progenitor reproducing previous results (Fig.4C,J) (Reiff et al 2015). Initially, we aimed to perform a full genetic epistatis analysis for *E75B* and *Kr-h1,* but this analysis was hampered as we failed to recombine *Kr-h1-RNAi* with *E75B* splice variant expression stocks.

However, we were able to analyze midguts of MF with simultaneous *>Kr-h1-RNAi*/*E75B-RNAi* (Fig.4D), which did not show any mating induction as could be expected from single *>Kr-h1*-RNAi (Reiff et al 2015). Forced *Kr-h1*-expression and simultaneous *E75B-RNAi* increase progenitor numbers with only few new EC (Fig.4E,F), supporting the necessity of *E75B* in EB differentiation (Fig.3E) and *Kr-h1* in ISC proliferation (Fig.4C). Surprisingly, we observed a strong increase of progenitor numbers forcing *Kr-h1* and *E75B-B* expression (Fig.4H,J). These results indicate an additive role of Ecdysone and JH-signaling on ISC proliferation forcing *E75B-B* and *Kr-h1*-expression, whereas the latter transduces the mating related proliferation response (Fig.3C).

Most interestingly, *E75B-A* and *–C*, despite of raised *Kr-h1*-levels, drive progenitors into EC differentiation largely phenocopying sole *E75B-A* and *-C* expression (compare Fig.3F,H and Fig.4G,I). Our data on *E75B-A* and *-C* corroborates a potent role for Ecdysone-induced EB differentiation. ISC fate decisions in the adult midgut rely on N-signaling (Micchelli & Perrimon 2006, Ohlstein & Spradling 2006, Ohlstein & Spradling 2007). During *Drosophila* follicle cell development N opposes EcR-function (Sun et al 2008), which prompted us to investigate *E75B-A/-C* as effectors of EcR-signaling in the context of N-dependent EB differentiation.

bioRxiv preprint doi: https://doi.org/10.1101/2020.02.24.962829; this version posted February 26, 2020. The copyright holder for this preprint (which was not certified by peer review) is the author/funder, who has granted bioRxiv a license to display the preprint in perpetuity. It is made available under aCC-BY 4.0 International license.

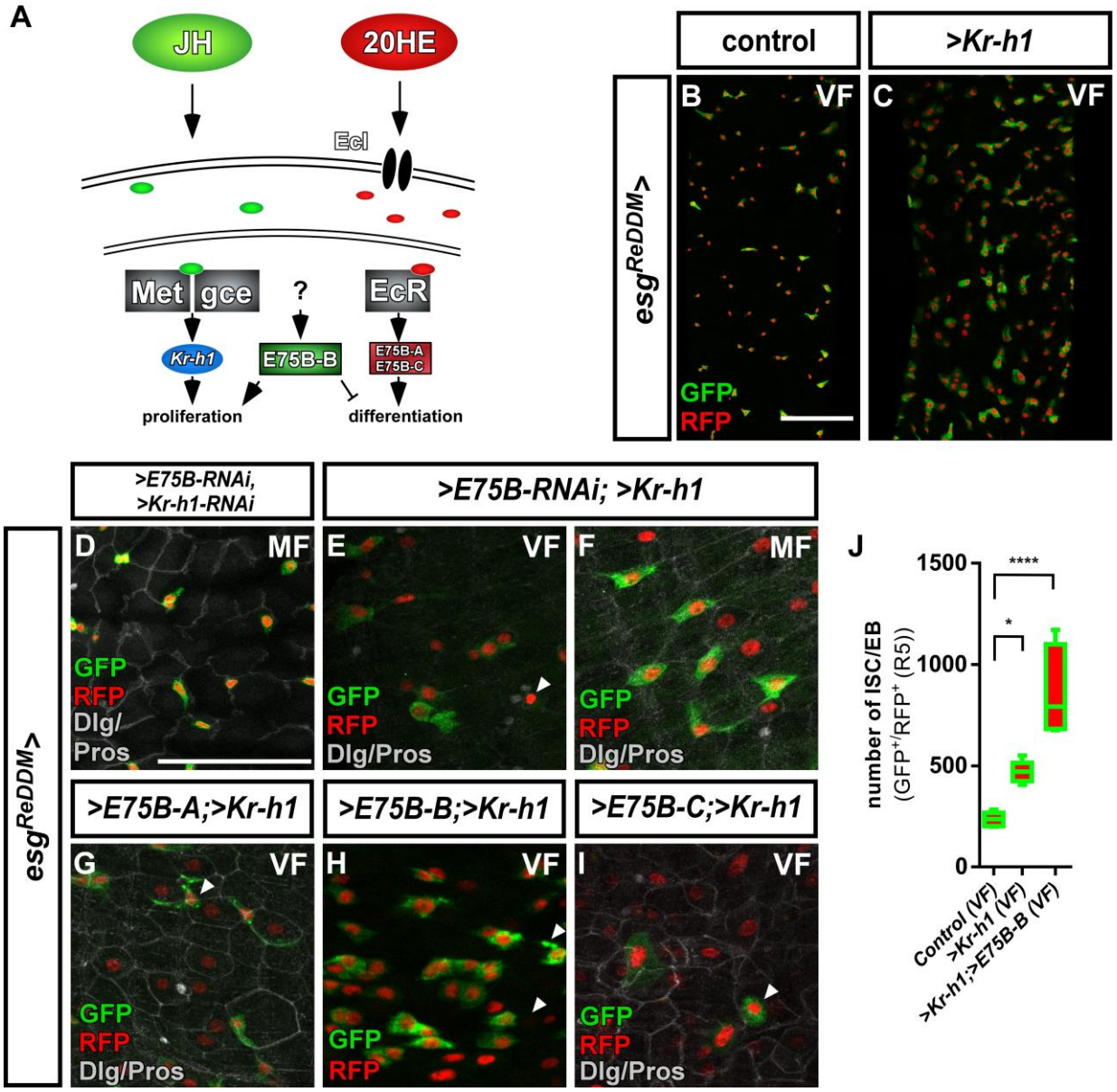

Figure 4. Crosstalk between JH- and Ecdysone-signalling pathways controlling intestinal progenitor proliferation and differentiation

(A) Cartoon depicting transcriptional effectors of JH- and Ecdysone signalling pathways. The JH receptor is formed by a heterodimer of *Methoprene tolerant (Met)* and *germ cells expressed (gce).* Ligand bound receptor activates the transcription of *krüppel homolog 1 (Kr-h1)* mediating mating effects in the adult intestine (Reiff et al 2015). (B-C) Images of adult PMG of control VF (B) and forced expression of *>Kr-h1* (C) traced for seven days with *esg*^{ReDDM}. Scale bars = 100µm. (D-I) Images of adult PMG with double *>E75-RNAi/>Kr-h1-RNAi* (D), forced expression of *>Kr-h1* with *>E75B-RNAi* in VF and MF (E,F) and expression of *E75B* splice variants *>E75B-A* (G)*, >E75B-B* (H) and *>E75B-C* (I) after seven days of tracing with *esg*^{ReDDM}. Please note that genotypes of (D-I) were accompanied with semi-lethality even at permissive 18°C, suggesting e.g. background transgene expression or position effects most probably caused by the total number of six transgenes including *esg*^{ReDDM}. PMG of *>Kr-h1* also showed some progenitor lethality indicated by membrane-blebbing and irregularities (arrowheads) as described in (Reiff et al 2019). (J) Quantification of progenitor numbers in R5 PMG (n=5,5,4). Error bars are Standard Error of the Mean (SEM) and asterisks denote significances from one-way ANOVA with Bonferroni's Multiple Comparison Test (* p<0.05, ** p<0.01; *** p<0,001; **** p<0.0001). Scale bars = 50µm

bioRxiv preprint doi: https://doi.org/10.1101/2020.02.24.962829; this version posted February 26, 2020. The copyright holder for this preprint (which was not certified by peer review) is the author/funder, who has granted bioRxiv a license to display the preprint in perpetuity. It is made available under aCC-BY 4.0 International license.

Ecdysone signaling overcomes Notch deficiency through *E75B-A* and *E75B-C* remote controlling enteroblast differentiation

In the *Drosophila* and mammalian intestinal stem cell niche, N-signaling specifies EE and EC fate (Jensen et al 2000, Micchelli & Perrimon 2006, Ohlstein & Spradling 2006, Ohlstein & Spradling 2007, VanDussen et al 2012). In *Drosophila*, *N* mutant ISC produce ISC-like progenitor cells and EE entirely lacking EC generation, resulting in an intestinal epithelium accumulating a lack of newly produced EC and compensatory proliferation (Fig.5A,B) (Chen et al 2018, Guo & Ohlstein 2015, Micchelli & Perrimon 2006, Ohlstein & Spradling 2006, Ohlstein & Spradling 2007, Patel et al 2015).

Using N-LOF tumors as an experimental paradigm lacking EC production, we sought to investigate the differentiation inducing properties of E75B-A/-C. Reduction of N by RNAi or a dominant-negative N-receptor using *esg^{ReDDM}* lead to tumors of different sizes, which we quantified and classified according to their number (Fig.5B). We predominantly found tumors of 5-10 cells (Fig.5B, S5A), but also few tumors containing more than 100 ISC/EE-like cells with indistinguishable single or multiple ISC origin (*class IV*, Fig.5B,S5A).

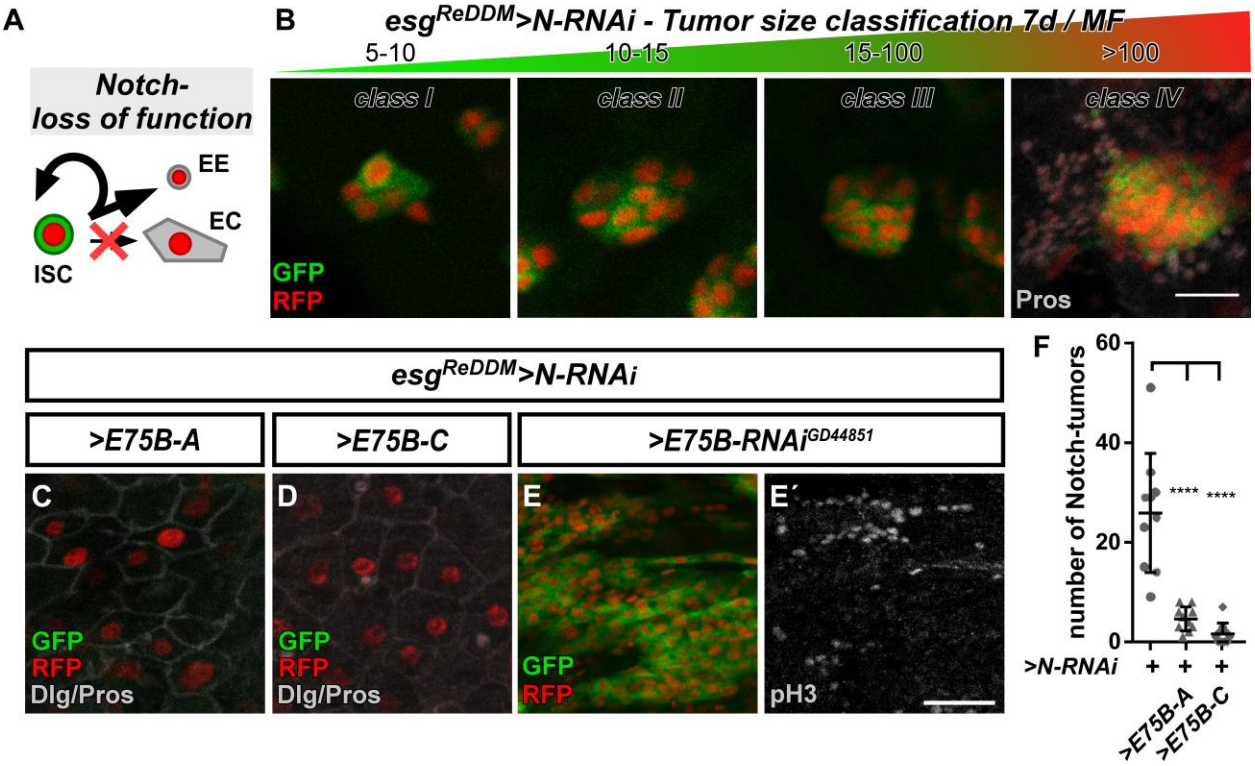

Figure 5 *Ecdysone induced protein 75B* controls ISC differentiation choices in a Notch tumor paradigm

(A) Cartoon depicting cell fate changes upon N-LOF combined with *esg^{ReDDM}* coloring (Ohlstein & Spradling 2006, Ohlstein & Spradling 2007). (B) *>N-RNAi* driven by *esg^{ReDDM}* leads to different tumor sizes after seven days of tracing that were classified in four classes according to size. Note, ISC-like/EE clusters up to four cells are not quantified as they occasionally occur in controls too. Progenitors are double labelled (GFP$^+$/RFP$^+$), where newly generated EE are identified by immunostaining for prospero (Pros) and H2B::RFP trace from *esg^{ReDDM}*. (C-D) Co- expression of *E75B* splice variants *>E75B-A* (C) and *>E75B-C* (D) after seven days of tracing with *esg^{ReDDM}>N-RNAi* in MF. Note additional Dlg-1$^+$-immunoreactivity in (grey,C+D) demonstrating epithelial integration of newly generated cells as EC (Dlg-1$^+$/RFP$^+$). (E+E') RNAi-mediated downregulation of *E75B* in MF shows confluent N-tumors (E) accompanied by increased mitosis (E'). (F) Quantification of ISC progeny encompassing ISC-like, EC and EE total tumor number in R5 PMG (n=10,10,10). Error bars are Standard Error of the Mean (SEM) and asterisks denote significances from one-way ANOVA with Bonferroni's Multiple Comparison Test (* p<0.05, ** p<0.01; *** p<0,001; **** p<0.0001). Scale bars = 100µm

bioRxiv preprint doi: https://doi.org/10.1101/2020.02.24.962829; this version posted February 26, 2020. The copyright holder for this preprint (which was not certified by peer review) is the author/funder, who has granted bioRxiv a license to display the preprint in perpetuity. It is made available under aCC-BY 4.0 International license.

Co-expression of *E75B-A/-C* with N-LOF strongly reduced total tumor number (Fig.5C,D,F) and smaller *class I*, *II* and *III* tumors (Fig.S5A), whereas *E75B-RNAi* results in confluent *class IV* tumors all along the PMG (Fig.5E). Although tumor number is strongly reduced (Fig.5F), occasional *class IV* tumors (<1/PMG) are able to escape suppressive E75B-A/-C showing no reduction in tumor size (Fig.S5A), suggesting that further tumorigenic mechanisms such as Upd- or EGF-ligands counteract the tumor suppressive function of 20HE signaling in *class IV* tumors (Patel et al 2015).

Since E75B-A and E75B-C re-enable EC differentiation despite the lack of N (Fig.5C,D Dlg-1^{+}/RFP^{+}), we investigated whether EcR-pathway activation is able to trigger EC fate in a N-LOF context. We activated EcR-signalling with RH5849 (Fig.6B) and raised intracellular levels of 20HE expressing *>EcI* in esg^{ReDDM}(Fig.6D). Either manipulation resulted in numerous confluent tumors reflecting the previously observed role of 20HE in proliferation (Fig.6F). In line with this, *>EcI-* and *>EcR-RNAi* significantly reduced tumor burden (Fig.6C,E,F).

More importantly, ecdysone-pathway activation led to significantly higher numbers of newly generated EC (arrowheads in Fig.6B,D,G), suggesting an upregulation of *E75B-A* and *E75B-C* in Notch tumors upon EcR-activation through RH5849 and *>EcI*. To exclude remaining N activity, we generated *N* mutant MARCM clones for *N* (N^{55e11}) (Guo & Ohlstein 2015). In agreement with our previous observations activating 20HE signaling in N clones led to a tenfold increase in EC numbers over controls (Fig.S6A-C) and forced expression of *>E75A/-C* to instant EC formation (Fig.S6D-E).

Taken together, our results implicate EcR-signaling in control of ISC proliferation, EB differentiation and metabolic adaptation of EC. Importantly, our data establishes 20HE as a systemic signal controlling reproductive adaptations in synergism with JH. Mating induced *E75B-A* and *E75B-C* act as differentiation effectors of EcR activity in EB inducing remote fate decisions. In neoplasms marked by a lack of fate specification (e.g. Notch-deficiency), our data suggests a new mechanism how steroid hormone signaling suppresses tumor growth by promoting post-mitotic cell fate.

bioRxiv preprint doi: https://doi.org/10.1101/2020.02.24.962829; this version posted February 26, 2020. The copyright holder for this preprint (which was not certified by peer review) is the author/funder, who has granted bioRxiv a license to display the preprint in perpetuity. It is made available under aCC-BY 4.0 International license.

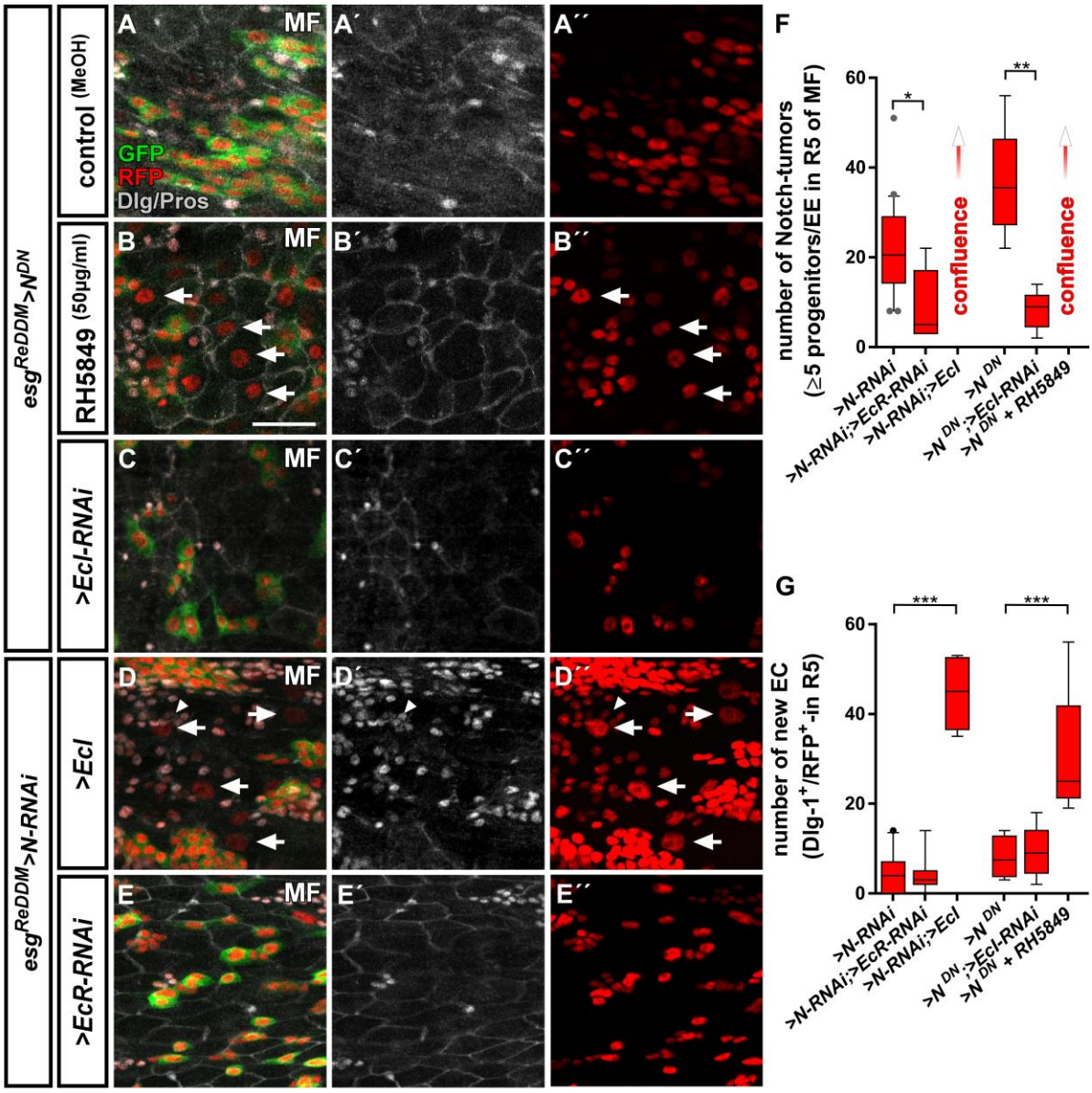

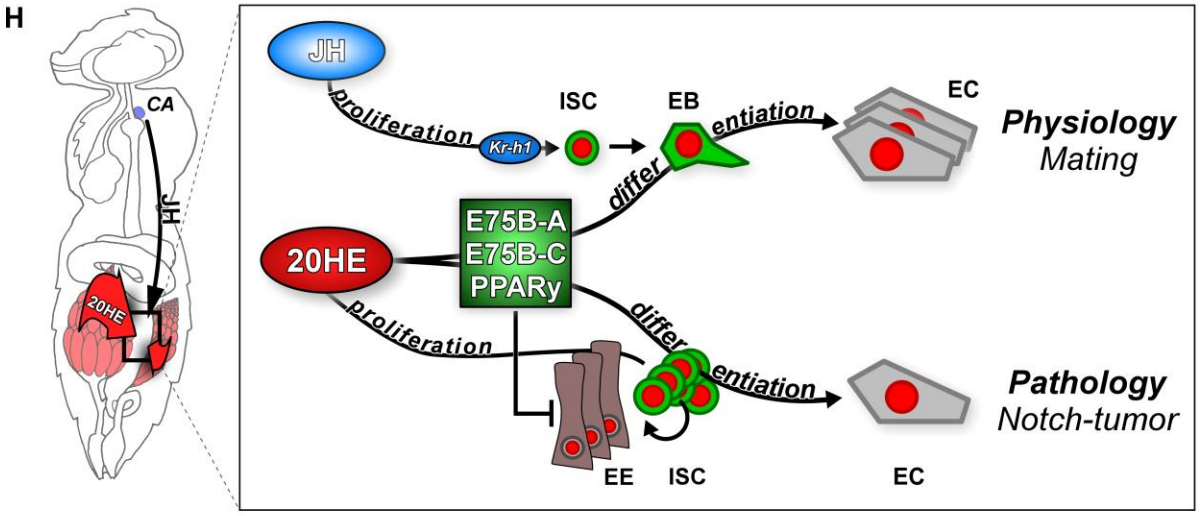

bioRxiv preprint doi: https://doi.org/10.1101/2020.02.24.962829; this version posted February 26, 2020. The copyright holder for this preprint (which was not certified by peer review) is the author/funder, who has granted bioRxiv a license to display the preprint in perpetuity. It is made available under aCC-BY 4.0 International license.

Figure 6. Ecdysone signaling re-enables EC-fate in a Notch tumor paradigm

(A-E'') Pharmacological and genetic manipulation of Ecdysone signalling. Adult PMG of MF with N-LOF (*>N-RNAi* or *>N^{DN}*) treated with MeOH as control (A-A'') or RH5849 (B-B'') to activate Ecdysone signalling. Arrowheads highlight newly generated Dlg-1^{+}/RFP^{+}-EC (B+B'') after seven days of *esg^{ReDDM}>N^{DN}*. (C-C'') RNAi-mediated downregulation of *EcI* in *esg^{ReDDM}>N^{DN}*, forced expression of *>EcI* (D-D'') and *>EcR-RNAi* (E-E'') in *esg^{ReDDM}>N-RNAi* MF after seven days of tracing. Arrowheads highlight newly generated Dlg-1^{+}-EC (D+D''), scale bars = 25µm. (F) Quantification of ISC progeny encompassing ISC-like, EC and EE classified after tumor size in R5 PMG (n=13,5,7,4,6,9). Error bars are Standard Error of the Mean (SEM) and asterisks denote significances from one-way ANOVA with Bonferroni's Multiple Comparison Test (* p<0.05, ** p<0.01; *** p<0,001; **** p<0.0001). (G) Quantification of newly generated EC (Dlg-1^{+}/RFP^{+}) in R5 PMG (n=13,5,7,4,6,9). Error bars are Standard Error of the Mean (SEM) and asterisks denote significances from one-way ANOVA with Bonferroni's Multiple Comparison Test (* p<0.05, ** p<0.01; *** p<0,001; **** p<0.0001). (H) Model of 20HE and JH hormonal pathways influencing physiological and pathological turnover in the intestine. Upon mating, JH from the neuroendocrine CA (*corpora allata*, (Reiff et al 2015)) as well as 20HE from the ovaries (this study) synergize on progenitor cells in the posterior midgut of adult female flies. JH induces ISC proliferation through Kr-h1, whereas 20HE signalling transduced by E75B-A/-C/PPARγ, ensures that newly produced EB differentiate into EC leading to a net increase in absorptive epithelium. In the adult intestine, early steps of tumorigenesis are recapitulated when EC fate is inhibited by the lack of Notch in progenitors. 20HE signalling through E75B-A/-C is capable to alleviate tumor growth by driving progenitors into post-mitotic EC fate.

Discussion

Systemic hormones and intestinal remodeling upon mating

Growing offspring involves significant metabolic adaptations to raised energy demands in mothers. *Drosophila melanogaster* uses a classical r-selected reproductive strategy with high number of offspring and minimal parental care (Pianka 1970). Upon mating, egg production is increased tenfold supported by metabolic and behavioral adaptations such as food intake and transit, nutrient preference and a net increase of absorptive tissue in the PMG depending on JH release (Carvalho et al 2006, Cognigni et al 2011, Reiff et al 2015, Ribeiro & Dickson 2010).

Here, we describe a role for the steroid-hormone ecdysone controlling intestinal tissue remodeling upon mating through EcR-signaling. The unliganded heterodimer of EcR and ultraspiracle (USP) binds its DNA consensus sequences serving as a repressor that turns into an activator upon ligand binding inducing early response genes *E74A, E75B* and *broad (br)* (Schwedes et al 2011, Uyehara & McKay 2019). Initially, we investigated knockdown of *USP, br* and *E74A* in intestinal progenitors and observed effects on progenitor survival independent of mating status (Fig.3C, Zipper and Reiff, *unpublished data*).

Our data supports the idea that 20HE and JH synergistically concert intestinal adaptations balancing nutrient uptake to increased energy demands upon mating (Fig.1-4). Mating induces ovarian ecdysteroid biosynthesis resulting in increased 20HE titers inducing egg production by ovarian GSC (Ables & Drummond-Barbosa 2010, Ameku & Niwa 2016, Ameku et al 2017, Harshman et al 1999, König et al 2011, Morris & Spradling 2012, Uyehara & McKay 2019). In the adjacent PMG, we describe the impact of ovarian 20HE on *E75B-A/-C* expression (Fig.6H) and show that 20HE import triggers EcR-activation: i) in VF with low ovarian 20HE levels, overexpression of wild-type *EcR* and *EcI* are unable to elicit neither ISC proliferation nor differentiation effects. ii) pharmacological activation using RH5849 as well as (iii) forced *EcI* expression strongly induce proliferation and EB differentiation in MF mediated by *E75B-A/-C*.

bioRxiv preprint doi: https://doi.org/10.1101/2020.02.24.962829; this version posted February 26, 2020. The copyright holder for this preprint (which was not certified by peer review) is the author/funder, who has granted bioRxiv a license to display the preprint in perpetuity. It is made available under aCC-BY 4.0 International license.

The interplay between *E75B* and *Kr-h1* controls intestinal size adaptation

Downstream of EcR, we found differential intestinal regulation of *E75B* splice variants upon mating. *E75B* activates egg production in ovarian GSC (Ables & Drummond-Barbosa 2010, König et al 2011, Morris & Spradling 2012, Uyehara & McKay 2019) and its knockdown reduces germarial size and number. In accordance with differentiation defects found in EB in our work, the number of cystoblasts, the immediate daughters of GSC, is reduced as well (Ables & Drummond-Barbosa 2010, Morris & Spradling 2012).

In our study, we dissected splice variant specific roles for *E75B* isoforms. *E75B-B* expression is at the lower detection limit and unchanged upon mating (Fig.3C). However, forced *E75B-B* expression raised ISC mitosis in VF (Fig.S4M). *E75B-B* mutants are viable and fertile and *E75B-B* is interacting with DNA only upon forming heterodimers with *Hormone receptor 3 (Hr3)* temporarily repressing gene expression (Bialecki et al 2002, Sullivan & Thummel 2003, White et al 1997). Further investigation of *E75B-B,* especially transcriptional regulation, is necessary to elucidate in which physiological context, else than mating, *E75B-B* controls ISC proliferation.

Mating induction of *E75B-A/-C,* but not *E75B-B,* suggests different transcriptional regulation. This idea is supported by the finding that larval epidermis from *Manduca sexta* exposed to heightened JH-levels is sensitized to 20HE, which results in a 10-fold increase of *E75B-A*, but not of *E75B-B* expression (Dubrovskaya et al 2004, Zhou et al 1998). An *in silico* analysis of 4kb regulatory regions upstream of *Kr-h1* using JASPAR revealed several EcR/USP and Met consensus sequences (Khan et al 2018), suggesting that both hormonal inputs may also converge on *Kr-h1* driving ISC proliferation (Fig.4D) (Reiff et al 2015). We propose a synergistic interplay between JH- and 20HE-signaling upon mating, in which the JH pathway effector *Kr-h1* increases proliferation in ISC and the EcR effectors *E75B-A*/-C drive EB into differentiation thereby ensuring mating induced organ size growth. The experimental investigation of *E75B* and *Kr-h1* regulatory regions incorporating endocrine signals from at least two different organs and leading to differential activity and function in ISC and EB will be a fascinating topic for future studies.

***E75B*/*PPARγ* and progenitor fate commitment in physiology and pathology**

A key discovery of our study is the role of *E75B-A/-C* in progenitor differentiation downstream of EcR activation. To our knowledge, this is the first time that N independent EB fate determination is reported. Notch signaling specifies EB as EC committed progenitors by the activation *klumpfuss* (Korzelius et al 2019, Reiff et al 2019). When tissue demand arises, EB are thought to physically separate from ISC and become independent of N. Detached EB acquire motility and are able to postpone their terminal epithelial integration after initial differentiation (Antonello et al 2015a, Antonello et al 2015b, Martin et al 2018, Siudeja et al 2015).

The ecdysone pathway acting through *E75B-A/-C* may provide such a signal for terminal EB differentiation, which is supported by several lines of evidence: i) EB-specific knockdown of *E75B* stalls their differentiation using klu^{ReDDM} (Fig.S4E), suggesting *E75B* activity after initial N-input. ii) klu^{+}-EB do not change fate upon *E75B* knockdown, suggesting a more mature EB differentiation status that already lost plasticity (Fig.S4A) (Korzelius et al 2019, Reiff et al 2019). iii) Forced *E75B-A/-C* expression in EB leads to their immediate differentiation independent of N-input (Fig.5C,D,S6D,E). Supporting an EB specific role, *E75B* was found to be highly expressed in progenitors in a recent study from the Perrimon lab (Hung et al 2018).

bioRxiv preprint doi: https://doi.org/10.1101/2020.02.24.962829; this version posted February 26, 2020. The copyright holder for this preprint (which was not certified by peer review) is the author/funder, who has granted bioRxiv a license to display the preprint in perpetuity. It is made available under aCC-BY 4.0 International license.

E75B is a long term predicted *PPARγ*-homologue *(peroxisome proliferator-activated receptor gamma)* in *Drosophila*, which got recently confirmed in pharmacogenetic approaches demonstrating that *E75B*-mutant flies are irresponsive to PPARγ activating drugs (Joardar et al 2015, King-Jones & Thummel 2005). This homology is of particular interest, as human PPARγ plays a role in i) pregnancy related adaptations of lipid metabolism (Waite et al 2000) and ii) as target in colorectal cancer (CRC) (Sarraf et al 1999).

Decreased PPARγ levels are associated with development of insulin resistance and failure of lipolysis in obese pregnant women (Rodriguez-Cuenca et al 2012, Vivas et al 2016). Here, we found an EcR-dependent upregulation of Srebp and PPARγ/E75B in adult female intestines that activate genes with known function in fatty acid synthesis and activation (Horton et al 2003, Reiff et al 2015, Seegmiller et al 2002). This interplay between SREBP, PPARγ and steroid hormone signaling needs to be dissected in detail to reveal to which extent adaptation of intestinal size and lipid metabolism contribute to pathophysiological conditions like diabetes.

In CRC, *PPARγ* loss-of-function mutations are observed in around 8% of patients (Sarraf et al 1999). *PPARγ* expression correlates with good prognosis and *PPARγ* is epigenetically silenced during CRC progression (Ogino et al 2009, Pancione et al 2010). In agreement with our *in vivo* experiments on E75B-A/-C in EB differentiation (Figs.3,5,6), *in vitro* studies identified *PPARγ* promoting differentiation in various colon cancer cell lines (Cesario et al 2006, Shimizu & Moriwaki 2008, Yamazaki et al 2007, Yoshizumi et al 2004).

In a CRC mouse model, biallelic loss of *PPARγ* leads to a 4-fold increase tumor incidence and reduced survival in female mice over males ($Apc^{Min/+}/PPAR\gamma^{-/-}$) (McAlpine et al 2006), whereas males develop around three times more colon tumors with wild type *PPARγ* (Cooper et al 2005). In line with this, ovariectomized $Apc^{Min/+}$ mice develop significantly more tumors and have decreased *PPARγ* expression, highlighting a possible link between *PPARγ* and estrogen signaling. Meta-analyses of hormone replacement studies have shown that estrogen confers a lower risk to develop CRC and better survival rates for female CRC patients (Chen et al 1998, Hendifar et al 2009, Lin et al 2012).

It is tempting to speculate that this mechanism of steroid hormones signaling through EcR/ER (estrogen receptor) to activate *E75B/PPARγ* is conserved from flies to humans. Indeed, human estradiol and 20HE activate the EcR with similar affinity and elicit *E75B* transcription by binding to *EcRE* (Ecdysone-Responsive Elements). *EcRE* can be converted to functional *ERE* (estrogen responsive elements) by a simple change of nucleotide spacing suggesting high conservation (Martinez et al 1991, Schwedes et al 2011).

Taken together, our findings reveal that mating induced steroid hormone release from the ovaries signal to adjacent intestinal stem cells controlling their proliferation and, more importantly, differentiation of committed precursor cells through *E75B/PPARγ.* Remote control of cell fate ensures absorptive epithelial cell production during mating related intestinal adaptations and in a *Drosophila* intestinal tumor model marked by loss of enterocyte fate specification. *E75B/PPARγ* acts independent of Notch-signaling, the only currently known precursor fate specifier in the intestinal stem cell niche. Mechanistically, we propose that *E75B/PPARγ* exerts an anti-neoplastic role by promoting progenitor differentiation into postmitotic enterocyte fate, thereby reducing the pool of mitotically active cells. Several studies describe pleiotropic roles for *PPARγ*. Combining knowledge about *PPARγ* protein structure and a distinct function of *PPARγ* in intestinal homeotasis may facilitate future studies using already available agonists and antagonists in the search for better treatment of colorectal cancer.

bioRxiv preprint doi: https://doi.org/10.1101/2020.02.24.962829; this version posted February 26, 2020. The copyright holder for this preprint (which was not certified by peer review) is the author/funder, who has granted bioRxiv a license to display the preprint in perpetuity. It is made available under aCC-BY 4.0 International license.

Acknowledgements

We thank Thomas Klein, Oren Schuldiner, Francois Schweisguth, Naoki Yamanaka, the Bloomington Drosophila Stock Center (NIHP400D018537), the Transgenic RNAi Project (TRiP) at Harvard Medical School (NIK/NIGMS R01-GM084947) and the Vienna Drosophila Resource Center (VDRC, http://www.vdrc.at) for providing transgenic fly stocks and Thomas Klein for being a very supportive host. We also thank Zeus Antonello, Nahuel Villegas, Hendrik Pannen and Thomas Klein for comments on the manuscript. The project is funded by a Deutsche Forschungsgesellschaft (DFG-Sachbeihilfe RE 34532-1) grant.

Material and Methods

Genetics and fly husbandry/ Fly strains

OregonR and w^{1118} flies served as wild-type controls. The following transgenes and mutations were employed: esg^{ReDDM} (Antonello et al 2015), klu^{ReDDM} (Reiff et al 2019), *UAS-EcI-Flag-HA* (Okamoto et al 2018), *UAS-EcI* (Okamoto et al 2018), *UAS-EcI-RNAi* (Okamoto et al 2018), *UAS-E75B-A-Flag* (Rabinovich et al 2016), *UAS-E75B-B-Flag* (Rabinovich et al 2016), *UAS-E75B-C-Flag* (Rabinovich et al 2016), $UAS\text{-}N^{DN}$ (J. Treisman), *Dl::GFP* (F. Schweisguth), N^{55e11} *FRT19A* (Guo & Ohlstein, 2015), *Srebp-GAL4* (Kunte et al 2006). From Bloomington (BDSC): *UAS-EcR-RNAi* (*BL58286*), *UAS-EcR.B2* (*BL4934*), $UAS\text{-}EcR.B2^{W650A}$ (BL9449), $UAS\text{-}EcR.B2^{F645A}$ (BL9450), EcR^{M554fs} (BL4894), *EcRE-lacZ (BL4516)*, $E75^{A81}$(BL23654), $E75^{07041}$ (BL11712), $E75^{\Delta 51}$ (BL23652), *UAS-CD8::GFP* (*BL5137*), ovo^{D1} (BL1309), *NRE::GFP* (*BL30727*), *NRE::GFP* (*BL30728*), From Kyoto: *UAS-Kr-h1* (DGRC120052). From FlyORF: $UAS\text{-}EcR\text{-}HA^{F000480}$, $UAS\text{-}Kr\text{-}h1^{F000495}$, $UAS\text{-}Met^{F000644}$, $UAS\text{-}gce^{F001915}$, From Vienna (VDRC) $UAS\text{-}EcR\text{-}RNAi^{GD37059}$, $UAS\text{-}E75B\text{-}RNAi^{GD44851}$, $UAS\text{-}E75B\text{-}RNAi^{KK108399}$, $UAS\text{-}N\text{-}RNAi^{GD14477}$, $UAS\text{-}Met\text{-}RNAi^{KK100638}$, $UAS\text{-}gce\text{-}RNAi^{KK101814}$.

Abbreviation	Genotype	In Figures
esgReDDM	w^{1118}; esg-GAL4, UAS-mCD8::GFP/+; $tub\text{-}GAL80^{ts}$, UAS-H2B::RFP/+	Fig.1-6
$esgReDDM>EcR\text{-}RNAi^{BL}$	w^{1118}; esg-GAL4, UAS-mCD8::GFP/$UAS\text{-}EcR\text{-}RNAi^{BL}$; $tub\text{-}GAL80^{ts}$, UAS-H2B::RFP/+	Fig.1; Fig.S1
$esgReDDM>EcR.B2^{wt}$	w^{1118}; esg-GAL4, UAS-mCD8::GFP/+; $tub\text{-}GAL80^{ts}$, UAS-H2B::RFP/UAS-EcR.B2	Fig.1
$esgReDDM>EcR^{F}$	w^{1118}; esg-GAL4, UAS-mCD8::GFP/+; $tub\text{-}GAL80^{ts}$, $UAS\text{-}H2B::RFP/UAS\text{-}EcR\text{-}HA^{F}$	Fig.1
EcRE-lacZ	y, w; EcRE-lacZ; +	Fig.1
ovo^{D1}; esgReDDM	ovo^{D1}/w^{1118}; esg-GAL4, UAS-mCD8::GFP/+; $tub\text{-}GAL80^{ts}$, UAS-H2B::RFP/+	Fig.2
esgReDDM>EcI	w^{1118}; esg-GAL4, UAS-mCD8::GFP/UAS-EcI; $tub\text{-}GAL80^{ts}$, UAS-H2B::RFP/+	Fig.2
esgReDDM>EcI-RNAi	w^{1118}; esg-GAL4, UAS-mCD8::GFP/+; $tub\text{-}GAL80^{ts}$, UAS-H2B::RFP/UAS-EcI-RNAi	Fig.2
WT/OregonR	+; +; +	Fig.3; Fig.S1
$esgReDDM>E75B\text{-}RNAi^{GD}$	w^{1118}; esg-GAL4, UAS-mCD8::GFP/$UAS\text{-}E75B\text{-}RNAi^{GD}$; $tub\text{-}GAL80^{ts}$, UAS-H2B::RFP/+	Fig.3
esgReDDM>E75B-A	w^{1118}; esg-GAL4, UAS-mCD8::GFP/ UAS-E75B-A-Flag; $tub\text{-}GAL80^{ts}$, UAS-H2B::RFP/+	Fig.3

bioRxiv preprint doi: https://doi.org/10.1101/2020.02.24.962829; this version posted February 26, 2020. The copyright holder for this preprint (which was not certified by peer review) is the author/funder, who has granted bioRxiv a license to display the preprint in perpetuity. It is made available under aCC-BY 4.0 International license.

esgReDDM>E75B-B	*w^{1118}; esg-GAL4, UAS-mCD8::GFP/ UAS-E75B-B-Flag; tub-$GAL80^{ts}$, UAS-H2B::RFP/+*	Fig.3
esgReDDM>E75B-C	*w^{1118}; esg-GAL4, UAS-mCD8::GFP/ UAS-E75B-C-Flag; tub-$GAL80^{ts}$, UAS-H2B::RFP/+*	Fig.3
esgReDDM>Met-RNAi^{KK} >EcR-RNAi^{BL}	*w^{1118}; esg-GAL4, UAS-mCD8::GFP/UAS-EcR-RNAi^{BL}; tub-$GAL80^{ts}$, UAS-H2B::RFP/UAS-Met-RNAi ^{KK}*	Fig.4
esgReDDM>gce-RNAi^{KK} >EcR-RNAi^{BL}	*w^{1118}; esg-GAL4, UAS-mCD8::GFP/UAS-EcR-RNAi^{BL}; tub-$GAL80^{ts}$, UAS-H2B::RFP/UAS-gce-RNAi ^{KK}*	Fig.4
esgReDDM>Met^{F}	*w^{1118}; esg-GAL4, UAS-mCD8::GFP/+; tub-$GAL80^{ts}$, UAS-H2B::RFP/UAS-Met^{F}*	Fig.4
esgReDDM>gce^{F}	*w^{1118}; esg-GAL4, UAS-mCD8::GFP/+; tub-$GAL80^{ts}$, UAS-H2B::RFP/UAS-gce^{F}*	Fig.4
esgReDDM>Kr-h1	*w^{1118}; esg-GAL4, UAS-mCD8::GFP/UAS-Kr-H1; tub-$GAL80^{ts}$, UAS-H2B::RFP/+*	Fig.4
*esgReDDM>E75B-*RNAi^{kk} >*Kr-H1*	*w^{1118}; esg-GAL4, UAS-mCD8::GFP/UAS-E75B-RNAi^{KK108399}; tub-$GAL80^{ts}$, UAS-H2B::RFP/UAS-Kr-H1*	Fig.4
esgReDDM>E75B-A >Kr-H1	*w^{1118}; esg-GAL4, UAS-mCD8::GFP/ UAS-E75B-A-Flag; tub-$GAL80^{ts}$, UAS-H2B::RFP/ UAS-Kr-H1*	Fig.4
esgReDDM>E75B-B >Kr-H1	*w^{1118}; esg-GAL4, UAS-mCD8::GFP/ UAS-E75B-B-Flag; tub-$GAL80^{ts}$, UAS-H2B::RFP/ UAS-Kr-H1*	Fig.4
esgReDDM>E75B-C >Kr-H1	*w^{1118}; esg-GAL4, UAS-mCD8::GFP/ UAS-E75B-C-Flag; tub-$GAL80^{ts}$, UAS-H2B::RFP/ UAS-Kr-H1*	Fig.4
esgReDDM>N-RNAi	*w^{1118}; esg-GAL4, UAS-mCD8::GFP/+; tub-$GAL80^{ts}$, UAS-H2B::RFP/UAS-N-RNAi*	Fig.5; Fig.6; Fig.S5
esgReDDM>E75B-A >N-RNAi	*w^{1118}; esg-GAL4, UAS-mCD8::GFP/UAS-E75B-A-Flag ; tub-$GAL80^{ts}$, UAS-H2B::RFP/UAS-N-RNAi*	Fig.5; Fig.S5
esgReDDM>E75B-B >N-RNAi	*w^{1118}; esg-GAL4, UAS-mCD8::GFP/UAS-E75B-B-Flag ; tub-$GAL80^{ts}$, UAS-H2B::RFP/UAS-N-RNAi*	Fig.5; Fig.S5
esgReDDM>E75B-C >N-RNAi	*w^{1118}; esg-GAL4, UAS-mCD8::GFP/UAS-E75B-C-Flag ; tub-$GAL80^{ts}$, UAS-H2B::RFP/UAS-N-RNAi*	Fig.5; Fig.S5
esgReDDM>E75B-RNAi^{GD} >N-RNAi	*w^{1118}; esg-GAL4, UAS-mCD8::GFP/UAS-E75B-RNAi^{GD} ; tub-$GAL80^{ts}$, UAS-H2B::RFP/UAS-N-RNAi*	Fig.5
esgReDDM>N^{DN}	*w^{1118}; esg-GAL4, UAS-mCD8::GFP/UAS-N^{DN}; tub-$GAL80^{ts}$, UAS-H2B::RFP/+*	Fig.6
esgReDDM>N^{DN} >EcI-RNAi	*w^{1118}; esg-GAL4, UAS-mCD8::GFP/UAS-N^{DN}; tub-$GAL80^{ts}$, UAS-H2B::RFP/UAS-EcI-RNAi*	Fig.6
esgReDDM>N-RNAi >EcI	*w^{1118}; esg-GAL4, UAS-mCD8::GFP/UAS-EcI; tub-$GAL80^{ts}$, UAS-H2B::RFP/UAS-N-RNAi*	Fig.6
esgReDDM>N-RNAi >EcR-RNAi^{BL}	*w^{1118}; esg-GAL4, UAS-mCD8::GFP/UAS-EcR-RNAi^{BL}; tub-$GAL80^{ts}$, UAS-H2B::RFP/UAS-N-RNAi*	Fig.6
Dl::GFP	*w^{1118}; +; DL::GFP/+*	Fig.S1
NRE::GFP	*$w^{1118;}$ NRE::GFP^{BL30727}/+; NRE::GFP^{BL30728}/+*	Fig.S1
esgReDDM>EcR.B2^{W650A}	*w^{1118}; esg-GAL4, UAS-mCD8::GFP/UAS-EcR.B2^{W650A}; tub-$GAL80^{ts}$, UAS-H2B::RFP/+*	Fig.S1
esgReDDM>EcR.B2^{F654A}	*w^{1118}; esg-GAL4, UAS-mCD8::GFP/+; tub-$GAL80^{ts}$, UAS-H2B::RFP/UAS-EcR.B2^{F654A}*	Fig.S1

bioRxiv preprint doi: https://doi.org/10.1101/2020.02.24.962829; this version posted February 26, 2020. The copyright holder for this preprint (which was not certified by peer review) is the author/funder, who has granted bioRxiv a license to display the preprint in perpetuity. It is made available under aCC-BY 4.0 International license.

esgReDDM/EcR^{M554fs}	*w^{1118}; esg-GAL4, UAS-mCD8::GFP/+; tub-GAL80^{ts}, UAS-H2B::RFP/EcR^{M554fs}*	Fig.S1
esgReDDM>EcR-RNAi^{GD}	*w^{1118}; esg-GAL4, UAS-mCD8::GFP/+; tub-GAL80^{ts}, UAS-H2B::RFP/UAS-EcR^{GD}*	Fig.S1
esgReDDM>EcI-Flag-HA	*w^{1118}; esg-GAL4, UAS-mCD8::GFP/UAS-EcI-Flag-HA; tub-GAL80^{ts}, UAS-H2B::RFP/+*	Fig.S2
Srebp>CD8::GFP	*w^{1118}; Srebp-Gal4, UAS-CD8::GFP, tub-GAL80^{ts}/+; +*	Fig.S2
Srebp>CD8::GFP >EcR-RNAi^{BL}	*w^{1118}; Srebp-Gal4, UAS-CD8::GFP, tub-GAL80^{ts}/UAS-EcR-RNAi^{BL}; +*	Fig.S2
MARCM (FRT2A)	*w^{1118}, hs-Flp, tub-GAL4, UAS-GFP^{nls}/w^{1118}; +; FRT2A, tub-GAL80/FRT2A*	Fig.S3
E75$^{\Delta 51}$-MARCM (FRT2A)	*w^{1118}, hs-Flp, tub-GAL4, UAS-GFP^{nls}/w^{1118}; +; FRT2A, tub-GAL80/FRT2A, E75$^{\Delta 51}$*	Fig.S3
E75^{A81}-MARCM (FRT2A)	*w^{1118}, hs-Flp, tub-GAL4, UAS-GFP^{nls}/w^{1118}; +; FRT2A, tub-GAL80/FRT2A, E75^{A81}*	Fig.S3
E75^{07041}-MARCM (FRT2A)	*w^{1118}, hs-Flp, tub-GAL4, UAS-GFP^{nls}/w^{1118}; +; FRT2A, tub-GAL80/FRT2A, E75^{07041}*	Fig.S3
kluReDDM	*w^{1118}; tub-GAL80^{ts}, UAS-mCD8::GFP/+; klu-GAL4, UAS-H2B::RFP/+*	Fig.S4
kluReDDM>EcR-RNAi^{BL}	*w^{1118}; tub-GAL80^{ts}, UAS-mCD8::GFP/UAS-EcR-RNAi^{BL}; klu-GAL4, UAS-H2B::RFP/+*	Fig.S4
kluReDDM>EcR-RNAi^{GD}	*w^{1118}; tub-GAL80^{ts}, UAS-mCD8::GFP/+; klu-GAL4, UAS-H2B::RFP/UAS-EcR-RNAi^{GD}*	Fig.S4
kluReDDM>E75B-A	*w^{1118}; tub-GAL80^{ts}, UAS-mCD8::GFP/UAS-E75B-A-Flag; klu-GAL4, UAS-H2B::RFP/+*	Fig.S4
kluReDDM>E75B-B	*w^{1118}; tub-GAL80^{ts}, UAS-mCD8::GFP/UAS-E75B-B-Flag; klu-GAL4, UAS-H2B::RFP/+*	Fig.S4
kluReDDM>E75B-C	*w^{1118}; tub-GAL80^{ts}, UAS-mCD8::GFP/UAS-E75B-C-Flag; klu-GAL4, UAS-H2B::RFP/+*	Fig.S4
N^{55e11}-MARCM (FRT19A)	*w^{1118} hsFlp, tubGAL80, FRT19A/w^{1118}, FRT19A, N^{55e11}; UAS-mCD8::GFP/+; tubGAL4/+*	Fig.S6
N^{55e11}-MARCM (FRT19A) ; >E75B-A	*w^{1118} hsFlp, tubGAL80, FRT19A/w^{1118}, FRT19A, N^{55e11}; UAS-mCD8::GFP/ UAS-E75B-A-Flag; tubGAL4/+*	Fig.S6
N^{55e11}-MARCM (FRT19A) ; >E75B-B	*w^{1118} hsFlp, tubGAL80, FRT19A/w^{1118}, FRT19A, N^{55e11}; UAS-mCD8::GFP/ UAS-E75B-B-Flag; tubGAL4/+*	Fig.S6
N^{55e11}-MARCM (FRT19A) ; >E75B-C	*w^{1118} hsFlp, tubGAL80, FRT19A/w^{1118}, FRT19A, N^{55e11}; UAS-mCD8::GFP/ UAS-E75B-C-Flag; tubGAL4/+*	Fig.S6
ovo^{D1}	*ovo^{D1}/+*	

MARCM clones

Mosaic analysis with a repressible cell marker (MARCM; Lee & Luo, 1999) clones were induced in midguts by Flippase under control of a *heat-shock* promoter. Expression of the Flippase was activated by 45 min in a 37°C-water bath to induce positively marked clones. The guts were dissected 5 days after induction. Clones in experimental and control flies were induced in parallel.

bioRxiv preprint doi: https://doi.org/10.1101/2020.02.24.962829; this version posted February 26, 2020. The copyright holder for this preprint (which was not certified by peer review) is the author/funder, who has granted bioRxiv a license to display the preprint in perpetuity. It is made available under aCC-BY 4.0 International license.

Food composition and fly keeping

Fly food contained 1424 g corn meal, 900 g malt extract, 800 g sugar beet syrup, 336 g dried yeast, 190 g soy fluor, 100 g agarose, 90 ml propionic acid and 30 g NIPAGIN powder (antimycotic agent) in 20 l H_2O. The food was cooked for about an hour to reduce bioburden, then filled into small plastic vials and cooled down at RT. Flies were kept at 25°C except for crosses with temperature-sensitive $GAL80^{ts}$ (GAL4 repressor) which were kept at 18°C (permissive temperature) until shifted to 29°C (restrictive temperature) to activate GAL4-mediated transgene expression. Crosses with esg^{ReDDM} and klu^{ReDDM} were carried out as described previously (Antonello et al., 2015; Reiff et al., 2015, 2018). Due to persisting problems with mucous formation on food surface in vials with virgin females, all experiments distinguishing between mated and virgin female flies were run on food with twice the amount of NIPAGIN. Mucous formation was avoided because of massive induction of tissue renewal by pathogenic stress.

Hormone analogue treatments

A vial of fly food was reheated in the microwave until it became liquid, the hormone analogues were added, thoroughly mixed and filled into a new vial. For each ml of food 5 µl of RH5849 (340 µM final concentration; 20 µg/µl stock solution, diluted in MeOH; DRE-C16813000, DrEhrenstorfer™) and/or 0.5 µl of Methoprene (1.49 mM final concentration; PESTANAL®, analytical standard; Sigma-Aldrich; Reiff et al., 2015) were added. As a control, an equivalent volume of carrier solution (MeOH) was added to the food. Hormone analogue treatments were performed for the period of the 7 days *ReDDM* (Antonello et al., 2015) shift.

Immunohistochemistry

Guts were dissected in PBS and were transferred into 4% PFA immediately after dissection. The staining was performed on an orbital shaker. After 45 min of fixation the guts were washed one time with PBS for 10 min. Antibodies were diluted in 0.5% PBT + 5% normal goat serum. The incubation with primary antibodies (1:250 anti-Dlg-1 [mouse; Developmental studies Hybridoma Bank (DSHB)]; 1:50 anti-Pros [mouse; DSHB]; 1:2000 anti-pH3 [rabbit; Merck Millipore, 06-570]; 1:50 anti-EcR common Ag10.2 [mouse; DSHB]; 1:500 anti-HA High Affinity 3F10 [rat; Merck, Sigma-Aldrich]) was performed at 4°C over night. After a second washing step with PBS the guts were incubated with secondary antibodies (1:500 Goat anti-MouseAlexa647 [Invitrogen]; 1:500 Goat anti-RatAlexa647 [Invitrogen]; 1:500 Goat anti-RabbitAlexa647 [Invitrogen]) and DAPI (1:1000; 100 µg/ml stock solution in 0.18 M Tris pH 7.4; DAPI No. 18860, Serva, Heidelberg) for at least 3 h at RT. Guts were washed a last time with PBS prior to mounting in Fluoromount-G™ Mounting Medium (Electron Microscopy Sciences, emsdiasum).

Image acquisition

Posterior midguts were imaged using an LSM 880 Airyscan confocal microscope (Carl Zeiss) using “Plan-Apochromat 10x/0.45 M27”, “Plan-Apochromat 20x/0.8 M27” and “C-Apochromat 40x/1.20 W Corr M27” objectives. Image resolution was set to at least 2048x2048 pixels. At least three focal planes (1 µm distance) were combined into a Z-stack to image one cell layer and to compensate for gut curvature.
For determining whole midgut length, an Axio Zoom.V16 (Carl Zeiss) was employed with DAPI filter and 1x/0.25-objective.

JASPAR

The open-access webtool JASPAR (Khan et al., 2018) was utilized to predict transcription factor binding sites within the 5’-UTR of *EcI*. It was specifically scanned for binding motifs related to Ecdysone and Juvenile Hormone signaling.

bioRxiv preprint doi: https://doi.org/10.1101/2020.02.24.962829; this version posted February 26, 2020. The copyright holder for this preprint (which was not certified by peer review) is the author/funder, who has granted bioRxiv a license to display the preprint in perpetuity. It is made available under aCC-BY 4.0 International license.

Quantification of proliferation and intensity measurements

Maximum intensity projections were calculated from Z-stack images of posterior midguts by Fiji (ImageJ 1.51n, Wayne Rasband, National Institutes of Health, USA). Total cell number and RFP-positive cell count of *ReDDM* (Antonello et al., 2015) guts were analyzed semi-automatically by a self-written macro for Fiji whereas GFP-positive cells were counted manually (available from the authors).

For fluorescence intensity measurements, intestines were scanned with fixed laser settings and measured in Fiji. The region of interest was selected manually and mean intensity of the area was determined. This way, relative EcR protein levels were measured in antibody stainings and relative SREBP activity was analyzed in PMG cells expressing *mCD8::GFP* under the control of *Srebp-GAL4*.

RNA isolation and cDNA synthesis

The R5 regions or ovaries of at least 3 female flies were dissected and transferred into a droplet of RNA*later*™ Solution (Invitrogen by Thermo Fisher Scientific) on ice. The tissue was homogenized in 100 µl peqGOLD TriFast (VWR Life Science) and total RNA was isolated as specified by the manufacturer. The following cDNA synthesis was performed with 250 ng of total RNA and the SuperScript™ IV Reverse Transcriptase (Invitrogen by Thermo Fisher Scientific) using a 1:1 mixture of oligo-dT primers and random hexamers directly upon RNA isolation. Prior to Real-time qPCR, cDNA samples were diluted 1:2 in dH_2O.

Verification of gene expression in the adult midgut by PCR

To verify gene expression in the adult *Drosophila* midgut, PCRs were performed with primer pairs specific for *ovo* or isoform-specific primer pairs for *EcR* spanning at least one exon-exon boundary. PCRs were performed with Q5® High-Fidelity DNA Polymerase (NEB) for at least 30 cycles. Reaction products were loaded on an agarose gel (1.5%) and separated by electrophoresis to verify lengths of PCR products.

Primer	Forward (5'-3')	Reverse (5'-3')
EcR.A	GGGGTCTAAGAAACATTTTGAGG	CCATTTGCAGCTGCAGCCGACGT
EcR.B1	GCACGTACGAAGCCCGATCGCGT	CCGGACTCGTTGCCGCAGAGCC
EcR.B2	GCACGTACGAAGCCCGATCGCGT	CTCTTCCCTCTGTTCACGCCC
ovo	CGCAGAGCCAAGATGTACGTG	GATAGTGGACCTCCGGCT

20-HE isolation and titer determination

20-HE titers were determined in VF and MF of the same age. Eclosed *OregonR* or heterozygous ovo^{D1} mutant flies were aged for 3d before mating. After 24 h or 48 h at least 20 adult female flies were pierced in the thorax with a needle and put into a 150 µl-PCR tube that was punctured in its very bottom. Hemolymph was harvested by centrifugation (5.000x g 5min RT) and collected in a 1.5 ml-reaction tube. Total weight of flies was determined before and after centrifugation. Typical yields of hemolymph were around 0.6-1 mg. The isolated hemolymph was mixed with 500 µl MeOH, centrifuged (12.000x g 20 min 4°C) and the supernatant was transferred into a new 1.5 ml-reaction tube. MeOH was evaporated at 30°C in a vacuum centrifuge (Eppendorf concentrator plus) and 20HE was resuspended in 100 µl EIA buffer and stored at -20°C until usage.

Ecdysone levels were determined using the 20-Hydroxyecdysone Enzyme Immunoassay kit according to manufacturer's instructions (#A05120.96 wells; Bertin Bioreagent). 20HE titer was normalized to hemolymph yield.

bioRxiv preprint doi: https://doi.org/10.1101/2020.02.24.962829; this version posted February 26, 2020. The copyright holder for this preprint (which was not certified by peer review) is the author/funder, who has granted bioRxiv a license to display the preprint in perpetuity. It is made available under aCC-BY 4.0 International license.

Real-time qPCR

Expression levels of Ecdysone signaling pathway-associated genes were determined in VF and MF. Eclosed *OregonR* or *EcRE-LacZ* flies were aged for 4d before mating. After 72 h of mating, RNA was isolated and cDNA synthetized before running qPCRs. After an enzyme activation step (20 sec 95°C), 40 cycles of denaturation (2 sec 95°C), primer annealing (20 sec 58°C) and elongation (20 sec 72°C) were run. Primers were designed to anneal at 59°C. Reaction was set up in technical triplicates with KAPA SYBR® FAST Universal (Roche) in a total volume of 10 µl. All qPCR results were normalized to the house-keeping gene *rp49* and include at least three biological replicates.

Primer	Forward (5'-3')	Reverse (5'-3')
E74A	AGAAACTTCGAGGCAATAGGGT	TGTGCGGCCTCATCTCAAG
E74B	TGGCCATCCCACAACGC	GGGCGGAAATGAACCTGTTG
E75B-A	CCTGTGCCAGAAGTTCGATGA	AAGAATCCATCGGCATCTTCGT
E75B-B	CGTCTAGCTCGATTCCTGATCTA	CGGAAGAATCCCTTGCAACC
E75B-C	CTGTGGTTCCGGCGGATT	TCGAATTCTATGTTGAGTTCTGGTT
EcR.A	GTGTTCGGTGAAAAACGCAA	TCCTAGCAACTGAGCTTTTGTAGAC
EcR.B1	TTAACGGTTGTTCGCTCGCA	AGTGCGGGAAACAATCAGAGCAT
EcR.B2	GTTAACGGTTGTTCGCTCGC	TGCGGGAAACAATCAGAGCATA
Kr-h1(A)	ACAATTTTATGATTCAGCCACAACC	GTTAGTGGAGGCGGAACCTG
Kr-h1(B)	AAATCTTGGGCACCCAAACAA	GTTGTGGCTGAATCTTTCGC
Lac-Z	ATCAGGATATGTGGCGGATGAGCG	AGTACAGCGCGGCTGAAATCATC
rp49	TGGTTTCCGGCAAGCTTCAA	TGTTGTCGATACCCTTGGGC

Statistical analysis

Quantifications were done as described in Antonello et al., 2015 and statistics were run in GraphPad Prism 6.01. For single comparisons, data sets were analyzed by two-sided unpaired t-test. For multiple comparisons, data sets were analyzed by one-way ANOVA and Tukey's post-hoc test. Significant differences are displayed as * for $p \leq 0.05$, ** for $p \leq 0.01$, *** for $p \leq 0.001$ and **** for $p \leq 0.0001$.

bioRxiv preprint doi: https://doi.org/10.1101/2020.02.24.962829; this version posted February 26, 2020. The copyright holder for this preprint (which was not certified by peer review) is the author/funder, who has granted bioRxiv a license to display the preprint in perpetuity. It is made available under aCC-BY 4.0 International license.

FIGURE LEGENDS

Figure 1. The Ecdysone receptor in intestinal progenitors controls tissue homeostasis

(A) Scheme of the adult *Drosophila melanogaster* gastrointestinal tract with cartoon depicting the midgut epithelial monolayer composed of intestinal stem cells (ISC), enteroblasts (EB), enterocytes (EC) and enteroendocrine cells (EE) colored according to the lineage tracing system ReDDM with esg-Gal4 (Antonello et al 2015a). *ReDDM* relies on two fluorescent transgenes with short- (membrane CD8::GFP, green) and long-term (nuclear H2B::RFP, red) stability and the ubiquitous Gal80 repressor (*tubα1-Gal80^{ts}*) for temporal control of UAS-driven transgenes (UAS abbreviated as > hereafter in Figure panels). Using *esg-Gal4*, the reporter transgenes are seen in the ISCs and EBs (GFP^+/RFP^+)). Over time, renewed ECs or EEs are traced by the nuclear RFP owing to the protein stability of H2B::RFP (Fig.S1) (Antonello et al., 2015). Posterior midguts (PMG) after seven days of *esg^{ReDDM}* tracing of control (crossed with *w^{1118}*) adult MF (C) show mating dependent addition of new EC compared to control VF (B) (Reiff et al 2015). (D) Knockdown of EcR using UAS-driven RNAi abolishes mating induced new EC generation in MF. (E+F) Overexpression of >*EcR.B2* in VF (E) and >*EcR^{FlyORF840}* (F) does not induce proliferation or differentiation of progenitors (ISC+EB). (G-I) Quantification of progenitor numbers (G) and traced progeny encompassing EC and EE (H) in R5 PMG (n=24,17,17,17, 8). Error bars are Standard Error of the Mean (SEM) and asterisks denote significances from one-way ANOVA with Bonferroni's Multiple Comparison Test (* p<0.05, ** p<0.01; *** p<0,001; **** p<0.0001). (I) Cartoon depicting experimental manipulations on EcR signalling pathway investigated with *esg^{ReDDM}*. Scale bars = 100µm

Figure 2. Intracellular 20-Hydroxy-ecdysone levels control ecdysone response through the ecdysone importer

(A+B) Representative adult PMG after seven days of *esg^{ReDDM}* tracing of control VF (A) and MF (B). (C) Control VF PMG after oral administration of RH5849 (50µg/ml) and seven days of tracing. (D-G) Up- and downregulation of *EcI* in VF (D,F) and MF (E,G) using UAS driven transgenes after seven days of tracing with *esg^{ReDDM}*. Quantitative RT-PCR on *EcRE* (Ecdysone responsive elements, (Schwedes et al 2011)) driving lacZ expression on intestinal cDNA from VF and MF control flies. Values are normalized to VF levels (horizontal line = 1) and statistically analysed using student´s t-test (* p<0.05, ** p<0.01; *** p<0,001;). (I) Cartoon depicting ovarian 20HE release and specific genetical and pharmacological manipulations on EcR signalling pathway in adjacent PMG ISC/EB. (J,K) Quantification of progenitor numbers (J) and traced progeny encompassing EC and EE (K) in R5 PMG (n=3,9,5,13/16,13,8,10,10,19). Error bars are Standard Error of the Mean (SEM) and asterisks denote significances from one-way ANOVA with Bonferroni's Multiple Comparison Test (* p<0.05, ** p<0.01; *** p<0,001; **** p<0.0001). Scale bars = 100µm

bioRxiv preprint doi: https://doi.org/10.1101/2020.02.24.962829; this version posted February 26, 2020. The copyright holder for this preprint (which was not certified by peer review) is the author/funder, who has granted bioRxiv a license to display the preprint in perpetuity. It is made available under aCC-BY 4.0 International license.

Figure 3. *Ecdysone induced protein 75B* is upregulated upon mating and controls progenitor differentiation

(A) Cartoon depicting EcR signalling cascade activating early ecdysteroid target genes. (B) Expression analysis of Ecdysone- and JH-signaling target genes including splice variants on cDNA transcribed from mRNA isolations from whole midgut dissections of MF. (C) Quantitative RT-PCR on early ecdysteroid genes on intestinal cDNA from VF and MF control flies. Values are normalized to VF levels (horizontal line = 1) and statistically analysed using student´s t-test (* p<0.05, ** p<0.01; *** p<0,001;). (D-E) RNAi-mediated downregulation of *E75B* in VF (D) and MF (E) after seven days of tracing with *esg*^{ReDDM}. (F-H) Representative images of adult PMG with forced expression of *E75B* splice variants *E75B-A* (F)*, E75B-B* (G) and *E75B-C* (H) after seven days of tracing with *esg*^{ReDDM}. Inset in (F) depicts epithelial integration of newly generated Dlg-1^{+}/RFP^{+}-EC. (I-J) Quantification of progenitor numbers (I) and traced progeny encompassing EC and EE (J) in R5 PMG (n=12,13,10,12,11,14,8,10,10,10). Error bars are Standard Error of the Mean (SEM) and asterisks denote significances from one-way ANOVA with Bonferroni's Multiple Comparison Test (* p<0.05, ** p<0.01; *** p<0,001; **** p<0.0001, identical p-values are marked by # when compared to MF). (K) Overall length in µm of midguts from proventriculus to mid-/hindgut boundary of indicated genotypes. Scale bars = 100µm

Figure 4. Crosstalk between JH- and Ecdysone-signalling pathways controlling intestinal progenitor proliferation and differentiation

(A) Cartoon depicting transcriptional effectors of JH- and Ecdysone signalling pathways. The JH receptor is formed by a heterodimer of *Methoprene tolerant (Met)* and *germ cells expressed (gce).* Ligand bound receptor activates the transcription of *krüppel homolog 1 (Kr-h1)* mediating mating effects in the adult intestine (Reiff et al 2015). (B-C) Images of adult PMG of control VF (B) and forced expression of *>Kr-h1* (C) traced for seven days with *esg*^{ReDDM}. Scale bars = 100µm. (D-I) Images of adult PMG with double *>E75-RNAi/>Kr-h1-RNAi* (D), forced expression of *>Kr-h1* with *>E75B-RNAi* in VF and MF (E,F) and expression of *E75B* splice variants *>E75B-A* (G)*, >E75B-B* (H) and *>E75B-C* (I) after seven days of tracing with *esg*^{ReDDM}. Please note that genotypes of (D-I) were accompanied with semi-lethality even at permissive 18°C, suggesting e.g. background transgene expression or position effects most probably caused by the total number of six transgenes including *esg*^{ReDDM}. PMG of *>Kr-h1* also showed some progenitor lethality indicated by membrane-blebbing and irregularities (arrowheads) as described in (Reiff et al 2019). (J) Quantification of progenitor numbers in R5 PMG (n=5,5,4). Error bars are Standard Error of the Mean (SEM) and asterisks denote significances from one-way ANOVA with Bonferroni's Multiple Comparison Test (* p<0.05, ** p<0.01; *** p<0,001; **** p<0.0001). Scale bars = 50µm

bioRxiv preprint doi: https://doi.org/10.1101/2020.02.24.962829; this version posted February 26, 2020. The copyright holder for this preprint (which was not certified by peer review) is the author/funder, who has granted bioRxiv a license to display the preprint in perpetuity. It is made available under aCC-BY 4.0 International license.

Figure 5 *Ecdysone induced protein 75B* controls ISC differentiation choices in a Notch tumor paradigm

(A) Cartoon depicting cell fate changes upon N-LOF combined with *esg^{ReDDM}* coloring (Ohlstein & Spradling 2006, Ohlstein & Spradling 2007). (B) *>N-RNAi* driven by *esg^{ReDDM}* leads to different tumor sizes after seven days of tracing that were classified in four classes according to size. Note, ISC-like/EE clusters up to four cells are not quantified as they occasionally occur in controls too. Progenitors are double labelled (GFP$^+$/RFP$^+$), where newly generated EE are identified by immunostaining for prospero (Pros) and H2B::RFP trace from *esg^{ReDDM}*. (C-D) Co- expression of *E75B* splice variants *>E75B-A* (C) and *>E75B-C* (D) after seven days of tracing with *esg^{ReDDM}>N-RNAi* in MF. Note additional Dlg-1$^+$-immunoreactivity in (grey,C+D) demonstrating epithelial integration of newly generated cells as EC (Dlg-1$^+$/RFP$^+$). (E+E') RNAi-mediated downregulation of *E75B* in MF shows confluent N-tumors (E) accompanied by increased mitosis (E'). (F) Quantification of ISC progeny encompassing ISC-like, EC and EE total tumor number in R5 PMG (n=10,10,10). Error bars are Standard Error of the Mean (SEM) and asterisks denote significances from one-way ANOVA with Bonferroni's Multiple Comparison Test (* p<0.05, ** p<0.01; *** p<0,001; **** p<0.0001). Scale bars = 100µm

Figure 6. Ecdysone signaling re-enables EC-fate in a Notch tumor paradigm

(A-E'') Pharmacological and genetic manipulation of Ecdysone signalling. Adult PMG of MF with N-LOF (*>N-RNAi* or *>N^{DN}*) treated with MeOH as control (A-A'') or RH5849 (B-B'') to activate Ecdysone signalling. Arrowheads highlight newly generated Dlg-1$^+$/RFP$^+$-EC (B+B'') after seven days of *esg^{ReDDM}>N^{DN}*. (C-C'') RNAi-mediated downregulation of *EcI* in *esg^{ReDDM}>N^{DN}*, forced expression of *>EcI* (D-D'') and *>EcR-RNAi* (E-E'') in *esg^{ReDDM}>N-RNAi* MF after seven days of tracing. Arrowheads highlight newly generated Dlg-1$^+$-EC (D+D''), scale bars = 25µm. (F) Quantification of ISC progeny encompassing ISC-like, EC and EE classified after tumor size in R5 PMG (n=13,5,7,4,6,9). Error bars are Standard Error of the Mean (SEM) and asterisks denote significances from one-way ANOVA with Bonferroni's Multiple Comparison Test (* p<0.05, ** p<0.01; *** p<0,001; **** p<0.0001). (G) Quantification of newly generated EC (Dlg-1$^+$/RFP$^+$) in R5 PMG (n=13,5,7,4,6,9). Error bars are Standard Error of the Mean (SEM) and asterisks denote significances from one-way ANOVA with Bonferroni's Multiple Comparison Test (* p<0.05, ** p<0.01; *** p<0,001; **** p<0.0001). (H) Model of 20HE and JH hormonal pathways influencing physiological and pathological turn-over in the intestine. Upon mating, JH from the neuroendocrine CA (*corpora allata*, (Reiff et al 2015)) as well as 20HE from the ovaries (this study) synergize on progenitor cells in the posterior midgut of adult female flies. JH induces ISC proliferation through Kr-h1, whereas 20HE signalling transduced by E75B-A/-C/PPARγ, ensures that newly produced EB differentiate into EC leading to a net increase in absorptive epithelium. In the adult intestine, early steps of tumorigenesis are recapitulated when EC fate is inhibited by the lack of Notch in progenitors. 20HE signalling through E75B-A/-C is capable to alleviate tumor growth by driving progenitors into post-mitotic EC fate.

bioRxiv preprint doi: https://doi.org/10.1101/2020.02.24.962829; this version posted February 26, 2020. The copyright holder for this preprint (which was not certified by peer review) is the author/funder, who has granted bioRxiv a license to display the preprint in perpetuity. It is made available under aCC-BY 4.0 International license.

SUPPLEMENTAL FIGURE LEGENDS

Figure S1 related to Figure 1

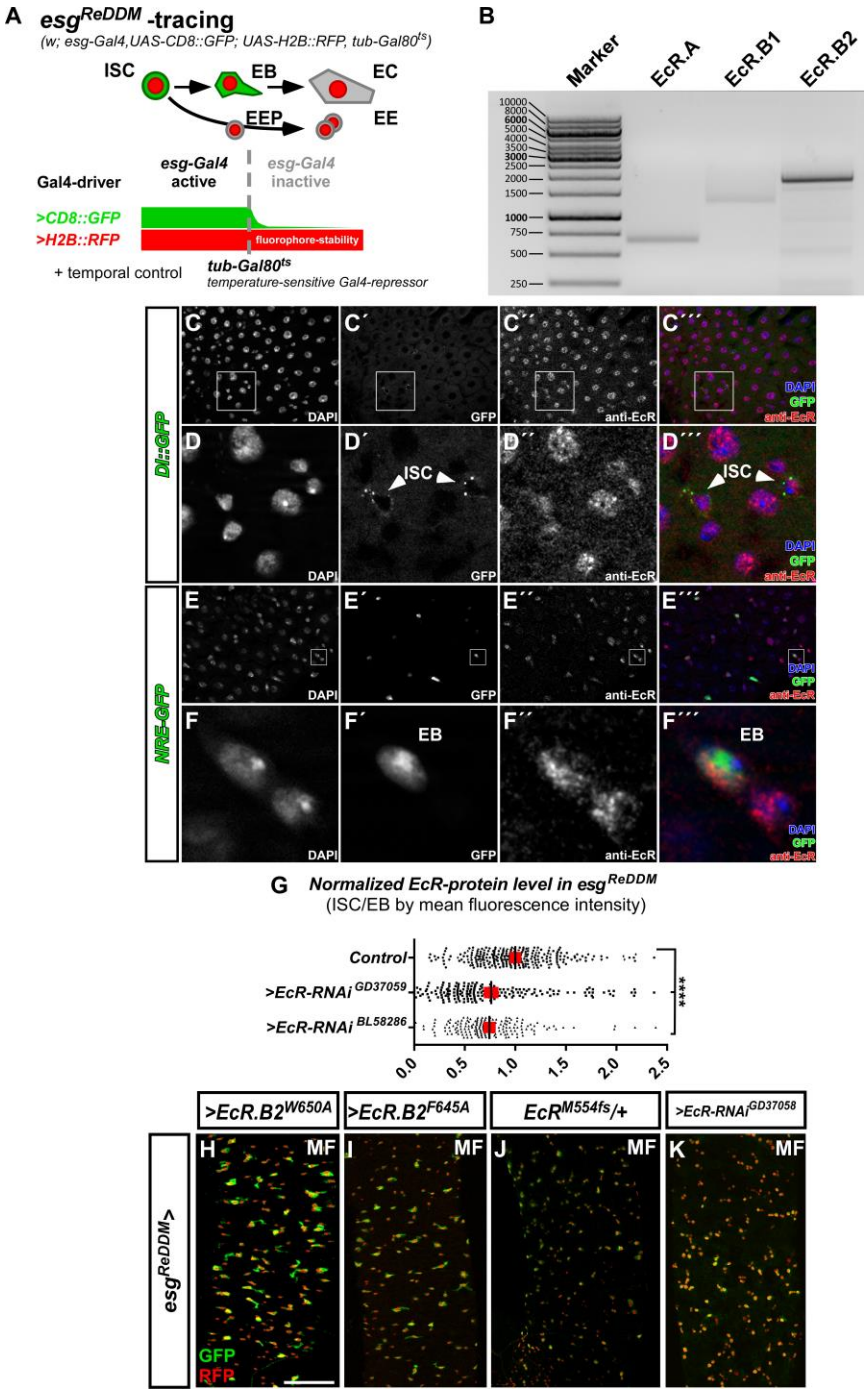

(A) Schematic of *esg*^{ReDDM} tracing including full genotype. *ReDDM* differentially marks cells having active or inactive *Gal4* expression. Combined with *esg-Gal4,* active in ISC and EB, *esg*^{ReDDM} double marks ISC and EB driving the expression of *UAS-CD8::GFP* and *UAS-H2B::RFP*, whereas newly differentiated EC and EE with inactive *esg-Gal4* are RFP^{+}-only. Flies are grown at permissive 18°C in which transgene expression is repressed by ubiquitous tubulin-driven Gal80^{ts}. By shifting adult females to the restrictive temperature of 29°C, Gal80^{ts} is destabilized, in turn enabling ReDDM-tracing marking progeny (EE and EC with H2B::RFP nuclear stain) and in parallel manipulation by allowing transactivation of UAS-sequences through *esg-driven* Gal4-expression (Antonello et al 2015a). (B) Expression analysis of Ecdysone-receptor splice variants with specific primer sets performed on cDNA transcribed from mRNA isolations of whole midgut dissections of adult MF. (C-F) Antibody staining against all EcR variants in PMG of adult MF using transgenic lines for the ISC-specific Notch-ligand Delta tagged with GFP (Dl::GFP, C-D''' inset magnification) and Notch responsive element marking EB (NRE-GFP, E-F''' inset magnification). Shown are single fluorescence channels including DAPI and merge (D'''-F'''). (G) *In situ* quantification of EcR levels by fluorescence intensity measurements in *esg*^{ReDDM} after seven days of tracing. Confocal images were taken at identical excitation and emission settings. Single GFP^{+}/RFP^{+} progenitor cell nuclei were measured using Fiji and statistically analyzed (n=272,179,179) using one-way ANOVA with Bonferroni's Multiple Comparison Test (* p<0.05, ** p<0.01; *** p<0,001; **** p<0.0001). (H-K) Forced expression of dominant-negative *EcR.B2*-variants (H+I), heterozygosity with the *EcR*^{M554fs}-allele (J) and a second *EcR-RNAi* (K) after seven days of *esg*^{ReDDM}-tracing in adult PMG of MF. Scale bars = 100µm

bioRxiv preprint doi: https://doi.org/10.1101/2020.02.24.962829; this version posted February 26, 2020. The copyright holder for this preprint (which was not certified by peer review) is the author/funder, who has granted bioRxiv a license to display the preprint in perpetuity. It is made available under aCC-BY 4.0 International license.

Figure S2 related to Figure 2

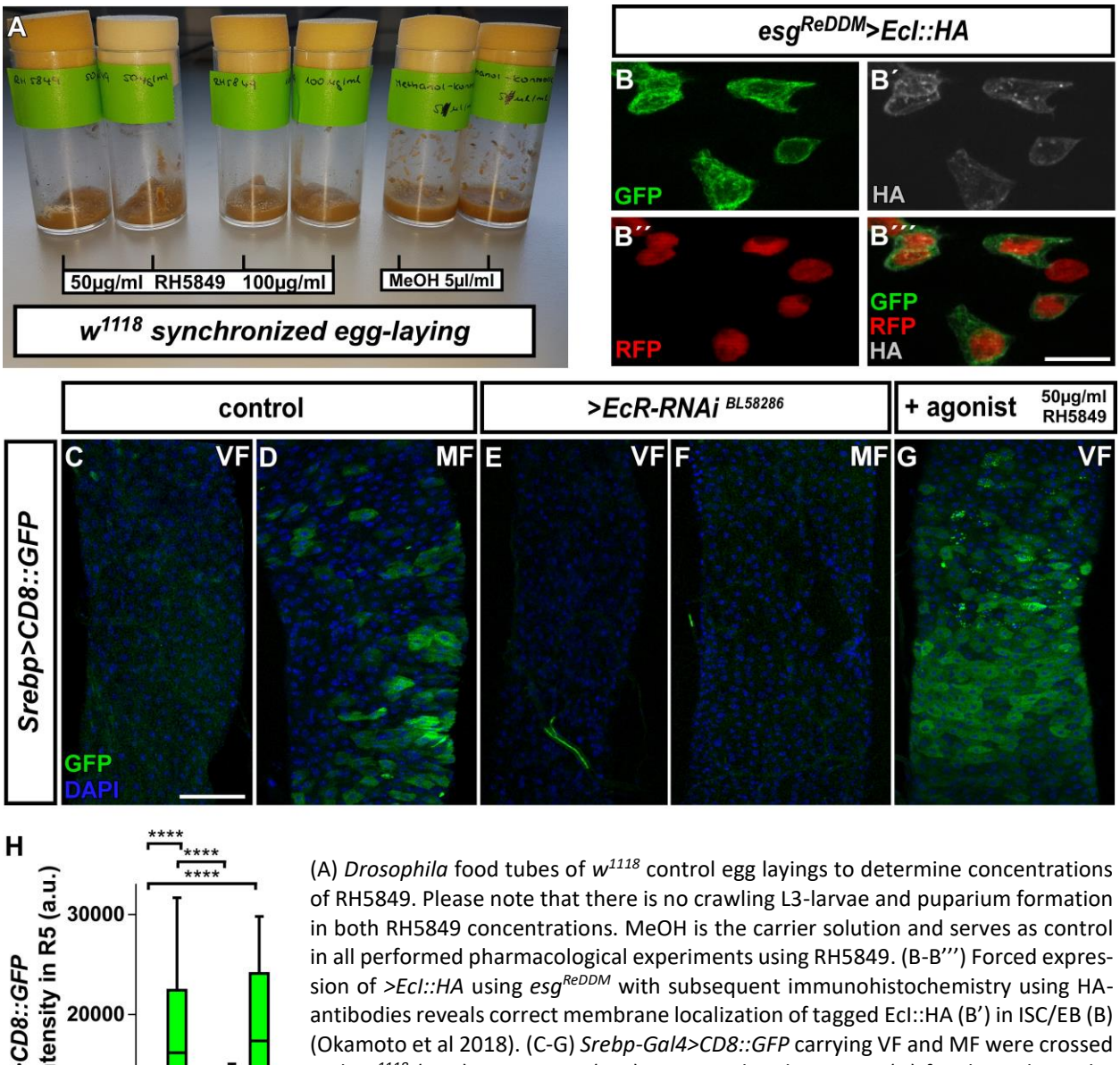

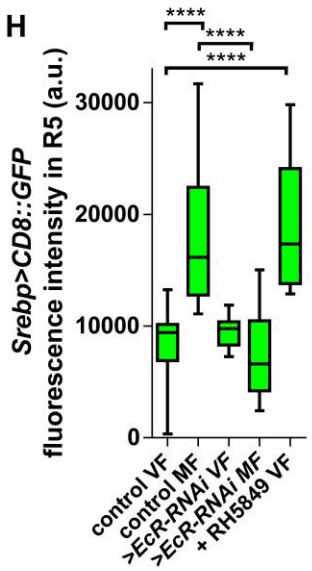

(A) *Drosophila* food tubes of w^{1118} control egg layings to determine concentrations of RH5849. Please note that there is no crawling L3-larvae and puparium formation in both RH5849 concentrations. MeOH is the carrier solution and serves as control in all performed pharmacological experiments using RH5849. (B-B''') Forced expression of *>EcI::HA* using esg^{ReDDM} with subsequent immunohistochemistry using HA-antibodies reveals correct membrane localization of tagged EcI::HA (B') in ISC/EB (B) (Okamoto et al 2018). (C-G) *Srebp-Gal4>CD8::GFP* carrying VF and MF were crossed with w^{1118} (C+D), *>EcR-RNAi* (E+F) or treated with RH5849 (G) for three days. The *Srebp-Gal4* line used is subjected to the same proteolytic processing as wild-type *Srebp*, thus reflecting upregulation of lipid uptake gene expression (Athippozhy et al 2011, Reiff et al 2015). (H) Mean GFP-fluorescence intensities in R5 PMG of according genotypes in (C-G) were measured using Fiji imaging software and statistically analyzed (n=12, 15, 13, 18, 9) using one-way ANOVA with Bonferroni's Multiple Comparison Test (* p<0.05, ** p<0.01; *** p<0,001; **** p<0.0001). Scale bars = 100µm

bioRxiv preprint doi: https://doi.org/10.1101/2020.02.24.962829; this version posted February 26, 2020. The copyright holder for this preprint (which was not certified by peer review) is the author/funder, who has granted bioRxiv a license to display the preprint in perpetuity. It is made available under aCC-BY 4.0 International license.

Figure S3 related to Figure 3

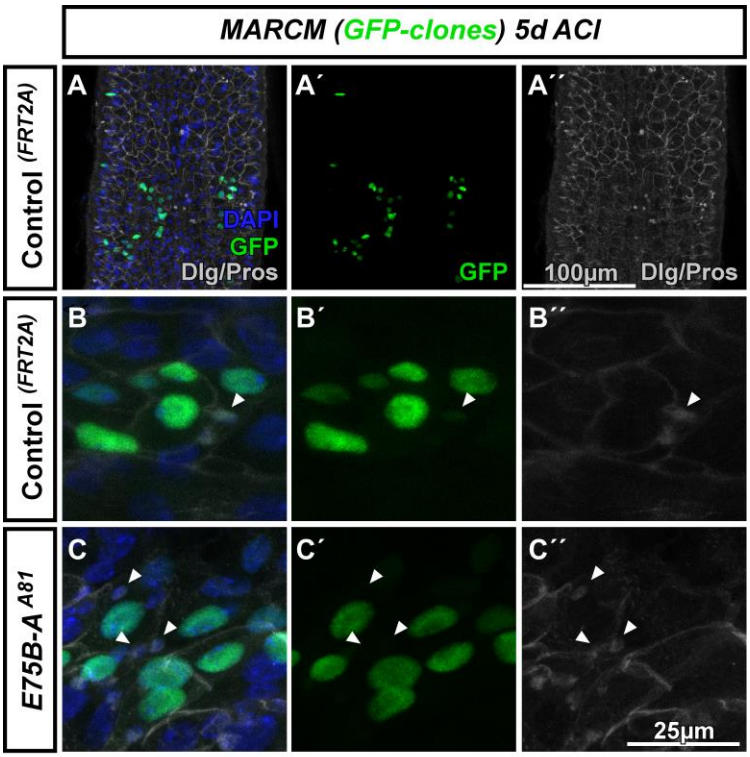

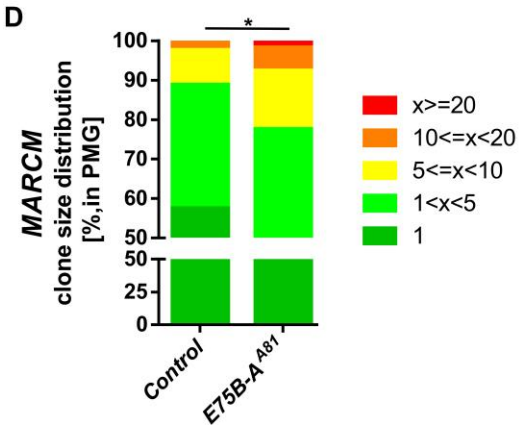

(A-E'') Representative images of MARCM clones of the indicated allele five days after clone induction (ACI) counterstained with Dlg-1 and Pros immunohistochemistry**.** Control clones lead to proper EC formation (big GFP$^+$-nuclei/Dlg-1$^+$) and EE (small GFP$^+$ diploid nuclei/Pros$^+$, arrowheads in B). *E75B-A* null mutant clones (C-C'') do not contain properly differentiated EC nor EE (arrowheads). Scale bars indicated in the images (A,B-C). (D) Quantification of GFP-MARCM clone size in R5 PMG (n=294,252 clones analyzed). Error bars are Standard Error of the Mean (SEM) and asterisks denote significances from unpaired Student´s t-test (* $p<0.05$).

bioRxiv preprint doi: https://doi.org/10.1101/2020.02.24.962829; this version posted February 26, 2020. The copyright holder for this preprint (which was not certified by peer review) is the author/funder, who has granted bioRxiv a license to display the preprint in perpetuity. It is made available under aCC-BY 4.0 International license.

Figure S4 related to Figure 3

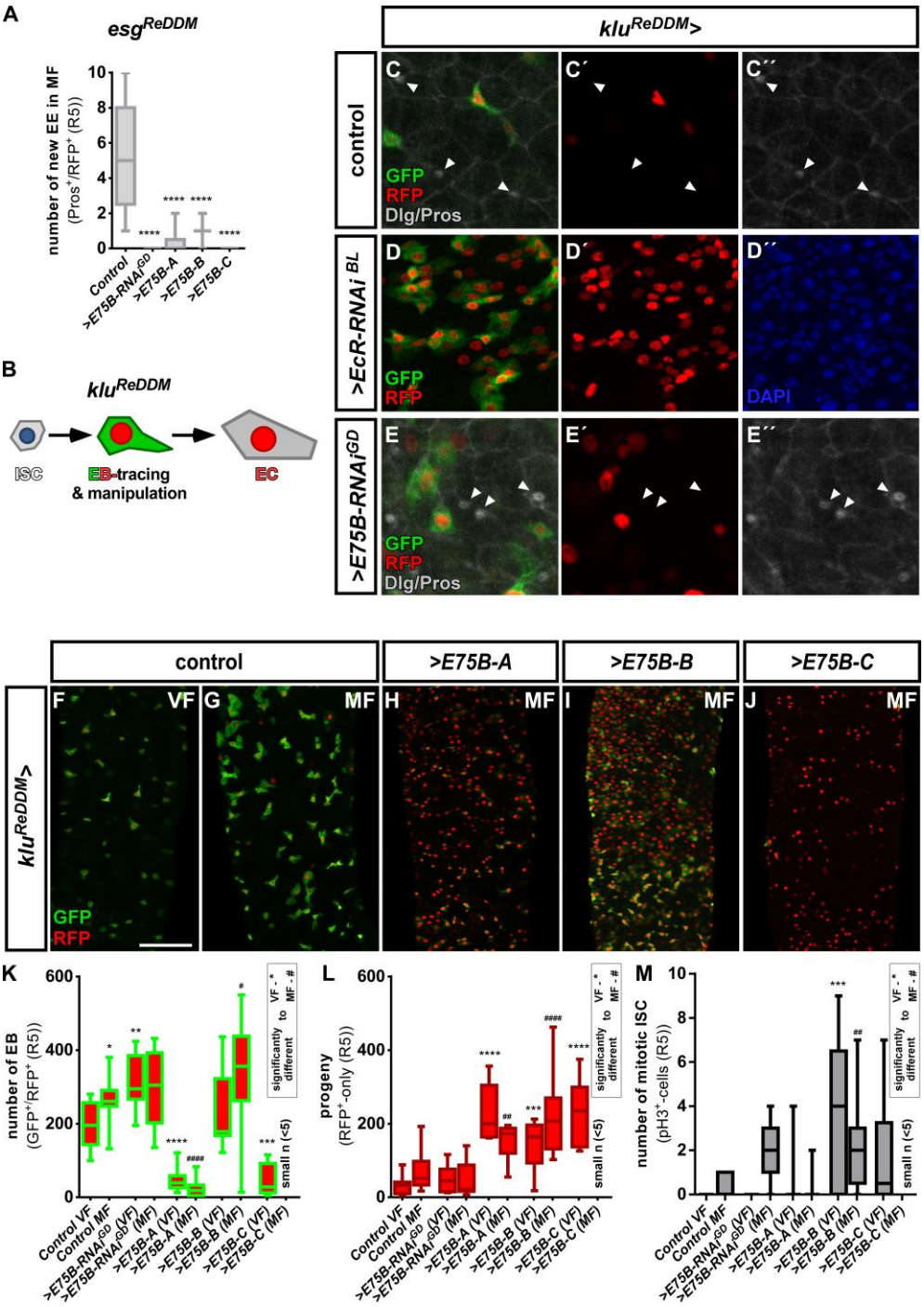

(A) Quantification of EE cells in R5 PMG (n=12,13,10,12,11). Error bars are Standard Error of the Mean (SEM) and asterisks denote significances from one-way ANOVA with Bonferroni's Multiple Comparison Test (* p<0.05, ** p<0.01; *** p<0,001; **** p<0.0001). (B) Cartoon depicting klu^{ReDDM}-tracing. *klu-Gal4* is active in EC-commited EB only and EC progeny is labelled with nuclear H2B::RFP (Reiff et al 2019). (C-E'') Representative images of MF controls (C-C'') and EB-specific knockdown of *EcR* (D-D´´) and *E75B* (E-E'') using klu^{ReDDM} after seven days of tracing. Differentiated progeny was identified in (C+E) with Dlg-1 and Pros immunohistochemistry. (F-J) Representative images of adult PMG of control VF (F) and MF (G) and forced expression of *E75B* splice variants *E75B-A* (H), *E75B-B* (I) and *E75B-C* (J) after seven days of tracing with klu^{ReDDM}. (K-M) Quantification of EB number (K), traced progeny encompassing EC and EE (L) and ISC mitosis (M) in R5 PMG (n=11,13,10,10,10,10,6,10,10,10). Error bars are Standard Error of the Mean (SEM) and asterisks denote significances from one-way ANOVA with Bonferroni's Multiple Comparison Test (* p<0.05, ** p<0.01; *** p<0,001; **** p<0.0001, identical p-values are marked by # when compared to MF). Scale bars = 100µm

bioRxiv preprint doi: https://doi.org/10.1101/2020.02.24.962829; this version posted February 26, 2020. The copyright holder for this preprint (which was not certified by peer review) is the author/funder, who has granted bioRxiv a license to display the preprint in perpetuity. It is made available under aCC-BY 4.0 International license.

Figure S5 related to Figure5

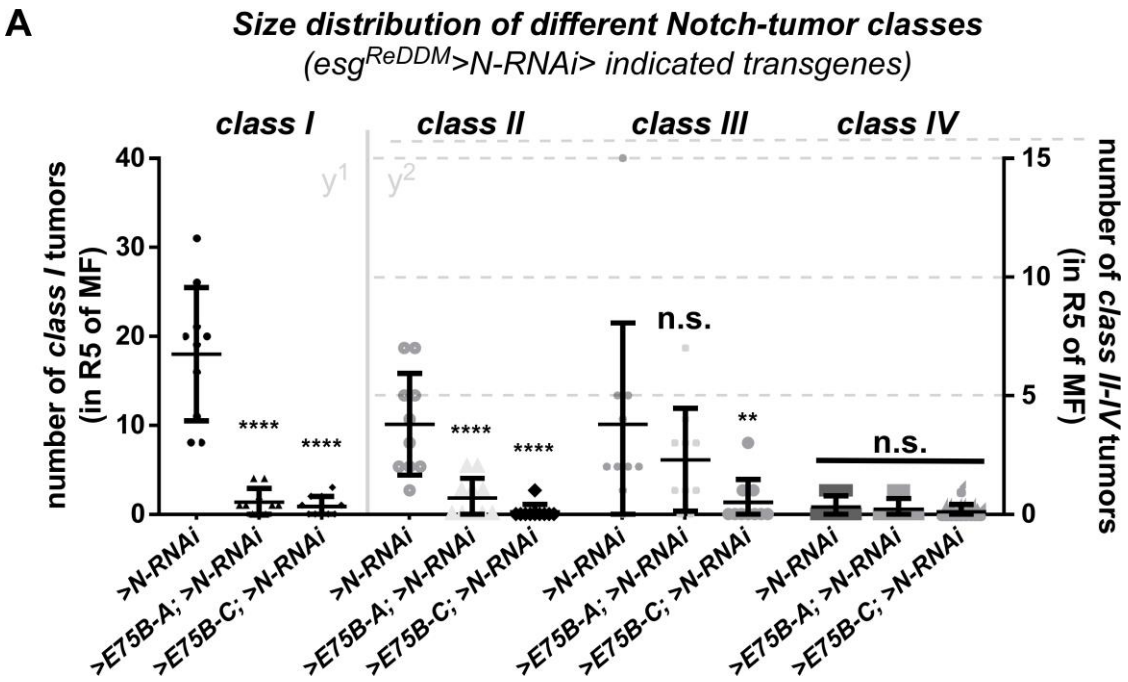

(A) Quantification of ISC progeny encompassing ISC-like, EC and EE classified after tumor size *(classes I to IV)* in R5 PMG of *esg^{ReDDM}>N-RNAi* (n=10,10,10). Error bars are Standard Error of the Mean (SEM) and asterisks denote significances from one-way ANOVA with Bonferroni's Multiple Comparison Test (* p<0.05, ** p<0.01; *** p<0,001; **** p<0.0001).

bioRxiv preprint doi: https://doi.org/10.1101/2020.02.24.962829; this version posted February 26, 2020. The copyright holder for this preprint (which was not certified by peer review) is the author/funder, who has granted bioRxiv a license to display the preprint in perpetuity. It is made available under aCC-BY 4.0 International license.

Figure S6 related to Figure 6

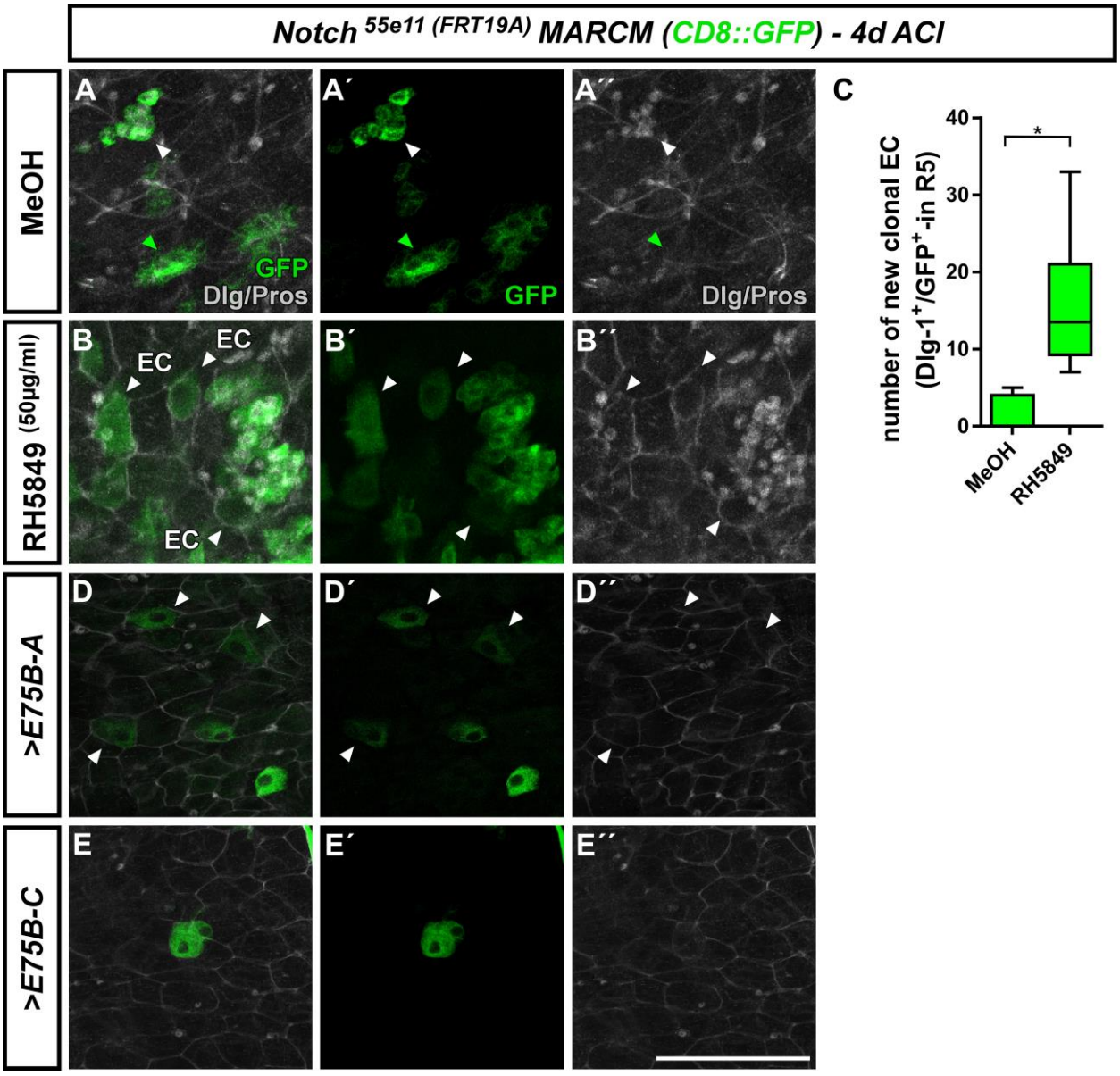

(A-E'') Representative images of MARCM clones for the Notch receptor (N^{55e11}) in MF PMG four days after clone induction (ACI) counterstained with Dlg-1 and Pros antibodies. Control *Notch* clones (MeOH) contain GFP-labelled clones containing ISC-like cells (GFP-only, green arrowheads) or EE (small GFP^+ diploid nuclei/$Pros^+$, white arrowheads). *Notch* null mutant clones (B-B'') treated with RH5849 contain differentiated EC in adjacent to Notch tumors ($Dlg1^+/GFP^+$) arrowheads). (C) Quantification of GFP-labelled EC part of and part of *Notch* MARCM clones in R5 PMG (n=7,6). Error bars are Standard Error of the Mean (SEM) and asterisks denote significances from unpaired Student´s t-test (* $p<0.05$, p=0,0129). (D+E) Forced expression of *>E75B-A* (D) and *>E75B-C* (E) leads to the immediate formation of single cell clones that immediately differentiated into EC (arrowheads). Scale bars = 100µm

bioRxiv preprint doi: https://doi.org/10.1101/2020.02.24.962829; this version posted February 26, 2020. The copyright holder for this preprint (which was not certified by peer review) is the author/funder, who has granted bioRxiv a license to display the preprint in perpetuity. It is made available under aCC-BY 4.0 International license.

Bibliography

Ables ET, Drummond-Barbosa D. 2010. The Steroid Hormone Ecdysone Functions with Intrinsic Chromatin Remodeling Factors to Control Female Germline Stem Cells in Drosophila. *Cell stem cell* 7: 581-92

Ameku T, Niwa R. 2016. Mating-Induced Increase in Germline Stem Cells via the Neuroendocrine System in Female Drosophila. *PLoS genetics* 12: e1006123

Ameku T, Yoshinari Y, Fukuda R, Niwa R. 2017. Ovarian ecdysteroid biosynthesis and female germline stem cells. *Fly (Austin)* 11: 185-93

Antonello ZA, Reiff T, Ballesta-Illan E, Dominguez M. 2015a. Robust intestinal homeostasis relies on cellular plasticity in enteroblasts mediated by miR-8-Escargot switch. *EMBO J* 34: 2025-41

Antonello ZA, Reiff T, Dominguez M. 2015b. Mesenchymal to epithelial transition during tissue homeostasis and regeneration: Patching up the Drosophila midgut epithelium. *Fly (Austin)* 9: 132-37

Athippozhy A, Huang L, Wooton-Kee CR, Zhao T, Jungsuwadee P, et al. 2011. Differential gene expression in liver and small intestine from lactating rats compared to age-matched virgin controls detects increased mRNA of cholesterol biosynthetic genes. *BMC Genomics* 12: 95

Bernardo TJ, Dubrovskaya VA, Xie X, Dubrovsky EB. 2014. A view through a chromatin loop: insights into the ecdysone activation of early genes in Drosophila. *Nucleic Acids Res* 42: 10409-24

Bialecki M, Shilton A, Fichtenberg C, Segraves WA, Thummel CS. 2002. Loss of the Ecdysteroid-Inducible E75A Orphan Nuclear Receptor Uncouples Molting from Metamorphosis in Drosophila. *Developmental Cell* 3: 209-20

Bownes M, D\"u b, Andreas, Smith T. 1984. Ecdysteroids in adult males and females of Drosophila melanogaster. *Journal of insect physiology* 30: 823-30

Carvalho GB, Kapahi P, Anderson DJ, Benzer S. 2006. Allocrine modulation of feeding behavior by the Sex Peptide of Drosophila. *Current biology : CB* 16: 692-6

Cesario RM, Stone J, Yen WC, Bissonnette RP, Lamph WW. 2006. Differentiation and growth inhibition mediated via the RXR:PPARgamma heterodimer in colon cancer. *Cancer Lett* 240: 225-33

Chen J, Xu N, Huang H, Cai T, Xi R. 2016. A feedback amplification loop between stem cells and their progeny promotes tissue regeneration and tumorigenesis. *eLife* 5: e14330

Chen J, Xu N, Wang C, Huang P, Huang H, et al. 2018. Transient Scute activation via a self-stimulatory loop directs enteroendocrine cell pair specification from self-renewing intestinal stem cells. *Nature cell biology* 20: 152-61

Chen MJ, Longnecker MP, Morgenstern H, Lee ER, Frankl HD, Haile RW. 1998. Recent use of hormone replacement therapy and the prevalence of colorectal adenomas. *Cancer Epidemiology Biomarkers & Prevention* 7: 227-30

Cherbas L, Hu X, Zhimulev I, Belyaeva E, Cherbas P. 2003. EcR isoforms in Drosophila: testing tissue-specific requirements by targeted blockade and rescue. *Development* 130: 271-84

Cognigni P, Bailey AP, Miguel-Aliaga I. 2011. Enteric neurons and systemic signals couple nutritional and reproductive status with intestinal homeostasis. *Cell metabolism* 13: 92-104

Cooper HS, Chang WC, Coudry R, Gary MA, Everley L, et al. 2005. Generation of a unique strain of multiple intestinal neoplasia (Apc(+/Min-FCCC)) mice with significantly increased numbers of colorectal adenomas. *Mol Carcinog* 44: 31-41

Dubrovskaya VA, Berger EM, Dubrovsky EB. 2004. Juvenile hormone regulation of the E75 nuclear receptor is conserved in Diptera and Lepidoptera. *Gene* 340: 171-7

Gilbert LI, Rybczynski R, Warren JT. 2002. Control and biochemical nature of the ecdysteroidogenic pathway. *Annual review of entomology* 47: 883-916

bioRxiv preprint doi: https://doi.org/10.1101/2020.02.24.962829; this version posted February 26, 2020. The copyright holder for this preprint (which was not certified by peer review) is the author/funder, who has granted bioRxiv a license to display the preprint in perpetuity. It is made available under aCC-BY 4.0 International license.

Gilbert LI, Warren JT. 2005. A molecular genetic approach to the biosynthesis of the insect steroid molting hormone. *Vitamins and hormones* 73: 31-57

Guo Z, Ohlstein B. 2015. Stem cell regulation. Bidirectional Notch signaling regulates Drosophila intestinal stem cell multipotency. *Science (New York, N.Y.)* 350: aab0988

Hammond KA. 1997. Adaptation of the maternal intestine during lactation. *Journal of mammary gland biology and neoplasia* 2: 243-52

Harshman LG, Loeb AM, Johnson BA. 1999. Ecdysteroid titers in mated and unmated Drosophila melanogaster females. *Journal of Insect Physiology* 45: 571-77

Hendifar A, Yang D, Lenz F, Lurje G, Pohl A, et al. 2009. Gender disparities in metastatic colorectal cancer survival. *Clinical cancer research : an official journal of the American Association for Cancer Research* 15: 6391-7

Horton JD, Shah NA, Warrington JA, Anderson NN, Park SW, et al. 2003. Combined analysis of oligonucleotide microarray data from transgenic and knockout mice identifies direct SREBP target genes. *Proceedings of the National Academy of Sciences* 100: 12027-32

Hudry B, Khadayate S, Miguel-Aliaga I. 2016. The sexual identity of adult intestinal stem cells controls organ size and plasticity. *Nature* 530: 344-48

Hung R-J, Hu C, Kirchner R, Li F, Xu C, et al. 2018. *A cell atlas of the adult Drosophila midgut*.

Jensen J, Pedersen EE, Galante P, Hald J, Heller RS, et al. 2000. Control of endodermal endocrine development by Hes-1. *Nat Genet* 24: 36-44

Jiang C, Baehrecke EH, Thummel CS. 1997. Steroid regulated programmed cell death during Drosophila metamorphosis. *Development* 124: 4673-83

Jiang C, Lamblin AF, Steller H, Thummel CS. 2000. A steroid-triggered transcriptional hierarchy controls salivary gland cell death during Drosophila metamorphosis. *Molecular cell* 5: 445-55

Jindra M, Palli SR, Riddiford LM. 2013. The Juvenile Hormone Signaling Pathway in Insect Development. *Annual Review of Entomology* 58: 181-204

Joardar A, Menzl J, Podolsky TC, Manzo E, Estes PS, et al. 2015. PPAR gamma activation is neuroprotective in a Drosophila model of ALS based on TDP-43. *Hum Mol Genet* 24: 1741-54

Karim FD, Thummel CS. 1991. Ecdysone coordinates the timing and amounts of E74A and E74B transcription in Drosophila. *Genes Dev* 5: 1067-79

Khan A, Fornes O, Stigliani A, Gheorghe M, Castro-Mondragon JA, et al. 2018. JASPAR 2018: update of the open-access database of transcription factor binding profiles and its web framework. *Nucleic Acids Research* 46: D260-D66

King-Jones K, Thummel CS. 2005. Nuclear receptors--a perspective from Drosophila. *Nature reviews. Genetics* 6: 311-23

Klepsatel P, Gáliková M, De Maio N, Ricci S, Schlötterer C, Flatt T. 2013. Reproductive and post-reproductive life history of wild-caught Drosophila melanogaster under laboratory conditions. *Journal of Evolutionary Biology* 26: 1508-20

König A, Yatsenko AS, Weiss M, Shcherbata HR. 2011. Ecdysteroids affect Drosophila ovarian stem cell niche formation and early germline differentiation. *The EMBO Journal* 30: 1549-62

Korzelius J, Azami S, Ronnen-Oron T, Koch P, Baldauf M, et al. 2019. The WT1-like transcription factor Klumpfuss maintains lineage commitment of enterocyte progenitors in the Drosophila intestine. *Nature Communications* 10: 4123

Kunte AS, Matthews KA, Rawson RB. 2006. Fatty acid auxotrophy in Drosophila larvae lacking SREBP. *Cell metabolism* 3: 439-48

Lee T, Luo L. 1999. Mosaic Analysis with a Repressible Cell Marker for Studies of Gene Function in Neuronal Morphogenesis. *Neuron* 22: 451-61

bioRxiv preprint doi: https://doi.org/10.1101/2020.02.24.962829; this version posted February 26, 2020. The copyright holder for this preprint (which was not certified by peer review) is the author/funder, who has granted bioRxiv a license to display the preprint in perpetuity. It is made available under aCC-BY 4.0 International license.

Lin BR, Huang MT, Chen ST, Jeng YM, Li YJ, et al. 2012. Prognostic significance of TWEAK expression in colorectal cancer and effect of its inhibition on invasion. *Annals of surgical oncology* 19 Suppl 3: S385-94

Martin JL, Sanders EN, Moreno-Roman P, Jaramillo Koyama LA, Balachandra S, et al. 2018. Long-term live imaging of the Drosophila adult midgut reveals real-time dynamics of division, differentiation, and loss. *eLife* 7: e36248

Martinez E, Givel F, Wahli W. 1991. *A common ancestor DNA motif for invertebrate and vertebrate hormone response element*. 263-8 pp.

McAlpine CA, Barak Y, Matise I, Cormier RT. 2006. Intestinal-specific PPARγ deficiency enhances tumorigenesis in ApcMin/+ mice. *International journal of cancer* 119: 2339-46

Micchelli CA, Perrimon N. 2006. Evidence that stem cells reside in the adult Drosophila midgut epithelium. *Nature* 439: 475-79

Miguel-Aliaga I, Jasper H, Lemaitre B. 2018. Anatomy and Physiology of the Digestive Tract of Drosophila melanogaster. *Genetics* 210: 357-96

Morris LX, Spradling AC. 2012. Steroid Signaling within Drosophila Ovarian Epithelial Cells Sex-Specifically Modulates Early Germ Cell Development and Meiotic Entry. *PLOS ONE* 7: e46109

Ogino S, Shima K, Baba Y, Nosho K, Irahara N, et al. 2009. Colorectal cancer expression of peroxisome proliferator-activated receptor gamma (PPARG, PPARgamma) is associated with good prognosis. *Gastroenterology* 136: 1242-50

Ohlstein B, Spradling A. 2006. The adult Drosophila posterior midgut is maintained by pluripotent stem cells. *Nature* 439: 470-74

Ohlstein B, Spradling A. 2007. Multipotent Drosophila intestinal stem cells specify daughter cell fates by differential notch signaling. *Science* 315: 988-92

Okamoto N, Viswanatha R, Bittar R, Li Z, Haga-Yamanaka S, et al. 2018. A Membrane Transporter Is Required for Steroid Hormone Uptake in Drosophila. *Dev Cell* 47: 294-305.e7

Pancione M, Sabatino L, Fucci A, Carafa V, Nebbioso A, et al. 2010. Epigenetic silencing of peroxisome proliferator-activated receptor gamma is a biomarker for colorectal cancer progression and adverse patients' outcome. *PLoS One* 5: e14229

Patel PH, Dutta D, Edgar BA. 2015. Niche Appropriation by Drosophila Intestinal Stem Cell Tumors. *Nature cell biology* 17: 1182-92

Pianka ER. 1970. On r- and K-Selection. *The American Naturalist* 104: 592-97

Rabinovich D, Yaniv SP, Alyagor I, Schuldiner O. 2016. Nitric Oxide as a Switching Mechanism between Axon Degeneration and Regrowth during Developmental Remodeling. *Cell* 164: 170-82

Reiff T, Antonello ZA, Ballesta-Illán E, Mira L, Sala S, et al. 2019. Notch and EGFR regulate apoptosis in progenitor cells to ensure gut homeostasis in Drosophila. *The EMBO Journal* 0: e101346

Reiff T, Jacobson J, Cognigni P, Antonello Z, Ballesta E, et al. 2015. Endocrine remodelling of the adult intestine sustains reproduction in Drosophila. *Elife* 4: e06930

Ribeiro C, Dickson BJ. 2010. Sex peptide receptor and neuronal TOR/S6K signaling modulate nutrient balancing in Drosophila. *Current biology : CB* 20: 1000-5

Roa J, Tena-Sempere M. 2014. Connecting metabolism and reproduction: Roles of central energy sensors and key molecular mediators. *Molecular and cellular endocrinology* 397: 4-14

Robinson P, Inwood M, Wilson I, Lafont R. 2008. *The metabolism of ingested and injected [3H]ecdysone by final instar larvae of Heliothis armigera*. 321-30 pp.

Robinson PD, Morgan ED, Wilson ID, Lafont R. 1987. The metabolism of ingested and injected [3H]ecdysone by final instar larvae of Heliothis armigera. *Physiological Entomology* 12: 321-30

Rodriguez-Cuenca S, Carobbio S, Velagapudi VR, Barbarroja N, Moreno-Navarrete JM, et al. 2012. Peroxisome proliferator-activated receptor gamma-dependent regulation of lipolytic nodes and metabolic flexibility. *Mol Cell Biol* 32: 1555-65

bioRxiv preprint doi: https://doi.org/10.1101/2020.02.24.962829; this version posted February 26, 2020. The copyright holder for this preprint (which was not certified by peer review) is the author/funder, who has granted bioRxiv a license to display the preprint in perpetuity. It is made available under aCC-BY 4.0 International license.

Sarraf P, Mueller E, Smith WM, Wright HM, Kum JB, et al. 1999. Loss-of-function mutations in PPAR gamma associated with human colon cancer. *Mol Cell* 3: 799-804

Schwedes C, Tulsiani S, Carney GE. 2011. Ecdysone receptor expression and activity in adult Drosophila melanogaster. *Journal of insect physiology* 57: 899-907

Seegmiller AC, Dobrosotskaya I, Goldstein JL, Ho YK, Brown MS, Rawson RB. 2002. The SREBP Pathway in Drosophila: Regulation by Palmitate, Not Sterols. *Developmental Cell* 2: 229-38

Segraves WA, Hogness DS. 1990. The E75 ecdysone-inducible gene responsible for the 75B early puff in Drosophila encodes two new members of the steroid receptor superfamily. *Genes Dev* 4: 204-19

Shimizu M, Moriwaki H. 2008. Synergistic Effects of PPARgamma Ligands and Retinoids in Cancer Treatment. *PPAR Res* 2008: 181047

Siudeja K, Nassari S, Gervais L, Skorski P, Lameiras S, et al. 2015. Frequent Somatic Mutation in Adult Intestinal Stem Cells Drives Neoplasia and Genetic Mosaicism during Aging. *Cell stem cell* 17: 663-74

Sullivan AA, Thummel CS. 2003. Temporal profiles of nuclear receptor gene expression reveal coordinate transcriptional responses during Drosophila development. *Mol Endocrinol* 17: 2125-37

Sun J, Smith L, Armento A, Deng W-M. 2008. Regulation of the endocycle/gene amplification switch by Notch and ecdysone signaling. *The Journal of cell biology* 182: 885-96

Talbot WS, Swyryd EA, Hogness DS. 1993. Drosophila tissues with different metamorphic responses to ecdysone express different ecdysone receptor isoforms. *Cell* 73: 1323-37

Uyehara CM, McKay DJ. 2019. Direct and widespread role for the nuclear receptor EcR in mediating the response to ecdysone in Drosophila. *Proceedings of the National Academy of Sciences of the United States of America* 116: 9893-902

VanDussen KL, Carulli AJ, Keeley TM, Patel SR, Puthoff BJ, et al. 2012. Notch signaling modulates proliferation and differentiation of intestinal crypt base columnar stem cells. *Development* 139: 488-97

Vivas Y, Díez-Hochleitner M, Izquierdo-Lahuerta A, Corrales P, Horrillo D, et al. 2016. Peroxisome proliferator activated receptor gamma 2 modulates late pregnancy homeostatic metabolic adaptations. *Molecular medicine (Cambridge, Mass.)* 22: 724-36

Waite LL, Person EC, Zhou Y, Lim K-H, Scanlan TS, Taylor RN. 2000. Placental Peroxisome Proliferator-Activated Receptor-γ Is Up-Regulated by Pregnancy Serum1. *The Journal of Clinical Endocrinology & Metabolism* 85: 3808-14

White KP, Hurban P, Watanabe T, Hogness DS. 1997. Coordination of Drosophila metamorphosis by two ecdysone-induced nuclear receptors. *Science* 276: 114-7

Wing KD, Slawecki RA, Carlson GR. 1988. RH 5849, a Nonsteroidal Ecdysone Agonist: Effects on Larval Lepidoptera. *Science* 241: 470-2

Yamazaki K, Shimizu M, Okuno M, Matsushima-Nishiwaki R, Kanemura N, et al. 2007. Synergistic effects of RXR alpha and PPAR gamma ligands to inhibit growth in human colon cancer cells--phosphorylated RXR alpha is a critical target for colon cancer management. *Gut* 56: 1557-63

Yoshizumi T, Ohta T, Ninomiya I, Terada I, Fushida S, et al. 2004. Thiazolidinedione, a peroxisome proliferator-activated receptor-gamma ligand, inhibits growth and metastasis of HT-29 human colon cancer cells through differentiation-promoting effects. *Int J Oncol* 25: 631-9

Zhou B, Hiruma K, Jindra M, Shinoda T, Segraves WA, et al. 1998. Regulation of the transcription factor E75 by 20-hydroxyecdysone and juvenile hormone in the epidermis of the tobacco hornworm, Manduca sexta, during larval molting and metamorphosis. *Dev Biol* 193: 127-38